The Astrophysical Journal, 875:59 (25pp), 2019 April 10 https://doi.org/10.3847/1538-4357/ab0e06

Optical Follow-up of Gravitational-wave Events during the Second Advanced LIGO/VIRGO Observing Run with the DLT40 Survey

Sheng Yang[1,2,3], David J. Sand[4], Stefano Valenti[1], Enrico Cappellaro[3], Leonardo Tartaglia[4,5], Samuel Wyatt[4], Alessandra Corsi[6], Daniel E. Reichart[7], Joshua Haislip[7], and Vladimir Kouprianov[7,8]
(DLT40 collaboration)

[1] Department of Physics, University of California, 1 Shields Avenue, Davis, CA 95616-5270, USA; sheng.yang@inaf.it
[2] Department of Physics and Astronomy Galileo Galilei, University of Padova, Vicolo dell'Osservatorio, 3, I-35122 Padova, Italy
[3] INAF Osservatorio Astronomico di Padova, Vicolo dell Osservatorio 5, I-35122 Padova, Italy
[4] Department of Astronomy/Steward Observatory, 933 North Cherry Avenue, Room N204, Tucson, AZ 85721-0065, USA
[5] Department of Astronomy and The Oskar Klein Centre, AlbaNova University Center, Stockholm University, SE-106 91 Stockholm, Sweden
[6] Physics & Astronomy Department,Texas Tech University, Lubbock, TX 79409, USA
[7] Department of Physics and Astronomy, University of North Carolina at Chapel Hill, Chapel Hill, NC 27599, USA
[8] Central (Pulkovo) Observatory of Russian Academy of Sciences, 196140 Pulkovskoye Avenue 65/1, Saint Petersburg, Russia
Received 2019 January 23; revised 2019 March 5; accepted 2019 March 6; published 2019 April 16

Abstract

We describe the gravitational-wave (GW) follow-up strategy and subsequent results of the Distance Less Than 40 Mpc survey (DLT40) during the second science run (O2) of the Laser Interferometer Gravitational-wave Observatory and Virgo collaboration (LVC). Depending on the information provided in the GW alert together with the localization map sent by the LVC, DLT40 would respond promptly to image the corresponding galaxies selected by our ranking algorithm in order to search for possible electromagnetic (EM) counterparts in real time. During the LVC O2 run, DLT40 followed 10 GW triggers, observing between ∼20 and 100 galaxies within the GW localization area of each event. From this campaign, we identified two real transient sources within the GW localizations with an appropriate on-source time—one was an unrelated SN Ia (SN 2017cbv), and the other was the optical kilonova, AT 2017fgo/SSS17a/DLT17ck, associated with the binary neutron star (BNS) coalescence GW170817 (a.k.a gamma-ray burst GRB 170817A). We conclude with a discussion of the DLT40 survey's plans for the upcoming LVC O3 run, which include expanding our galaxy search fields out to $D \approx 65$ Mpc to match the LVC's planned three-detector sensitivity for BNS mergers.

Key words: gravitational waves – methods: observational – supernovae: general

1. Introduction

The long-awaited direct detection of gravitational waves (GWs) by first the Advanced Laser Interferometer Gravitational-wave Observatory (LIGO; Aasi et al. 2015) and then the Advanced Virgo interferometer (Acernese et al. 2015) has ushered in a new era of physics. These exquisite detectors are designed to probe high-frequency (∼10–1000 Hz) GW signals whose main astrophysical sources are compact binary coalescences (CBCs)—i.e., binary black hole (BBH), black hole—neutron star, and binary neutron star (BNS) mergers.

During the first Advanced LIGO observing run (O1), two BBH GW events were detected (GW150914; Abbott et al. 2016a, and GW151226; Abbott et al. 2016b), along with a third likely event of astrophysical origin (LVT151012; Abbott et al. 2016c). While BBH mergers are not generally expected to have electromagnetic (EM) counterparts,[9] the astronomical community (joined by neutrino and cosmic-ray researchers) promptly responded and searched for transients associated with these BBH events (see, e.g., Abbott et al. 2016d, for a summary of the follow-up of GW150914), partly in preparation for GW events that are expected to have an EM counterpart, namely those with a neutron star as one of the constituents.

The participation of the EM, neutrino, and cosmic-ray communities continued in the second LVC observing season (O2), with hundreds of telescopes and detectors participating in the follow-up of GW sources. During O2, the Advanced LIGO detectors were significantly more sensitive, and were joined by Virgo in the final month of data taking—this is significant, as the addition of a third detector can decrease the GW localization regions from ∼100–1000 deg^2 to ∼10–100 deg^2 for high-signal-to-noise events (Abbott et al. 2018). In total, 14 GW alerts were issued by the LVC, 6 of which were ultimately determined to be true GW events (The LIGO Scientific Collaboration & the Virgo Collaboration 2019). Many of these were aggressively pursued by the astronomical community, whose efforts finally bore fruit with the GW170817 BNS merger (Abbott et al. 2017a), which led to the discovery of the first EM counterpart of a GW event (from gamma-ray to radio wavelengths; Abbott et al. 2017b; Arcavi et al. 2017a; Coulter et al. 2017; Goldstein et al. 2017; Haggard et al. 2017; Hallinan et al. 2017; Lipunov et al. 2017; Margutti et al. 2017; Savchenko et al. 2017; Soares-Santos et al. 2017; Tanvir et al. 2017; Troja et al. 2017; Valenti et al. 2017).

In this paper, we describe the observational campaign performed by the Distance Less Than 40 Mpc (DLT40) project and its GW follow-up efforts during the LVC O2 run. Elsewhere, we have described the codiscovery of AT2017gfo/SSS17a/DLT17ck and

[9] Whether a BBH merger can produce an EM signal is still an open question. A weak gamma-ray transient was reported 0.4 s after GW150914, consistent with the GW localization (Connaughton et al. 2016). Subsequent models and theoretical work (Loeb 2016; Perna et al. 2016, 2018; Zhang et al. 2016; Bartos et al. 2017; de Mink & King 2017) make the continued search for EM counterparts to BBHs a source of interest.

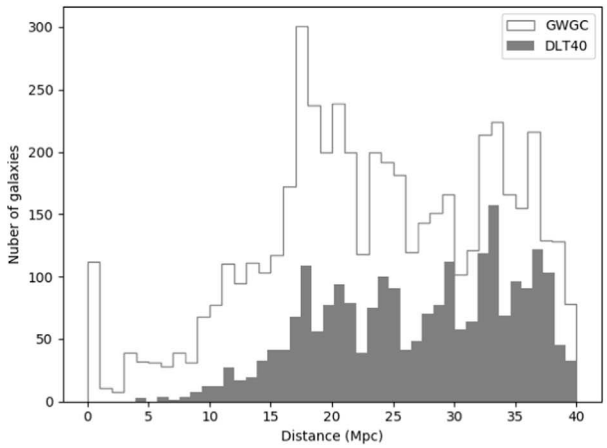

(a) The distance distribution of DLT40 (filled histogram) and GWGC galaxies within 40 Mpc (shaded histogram).

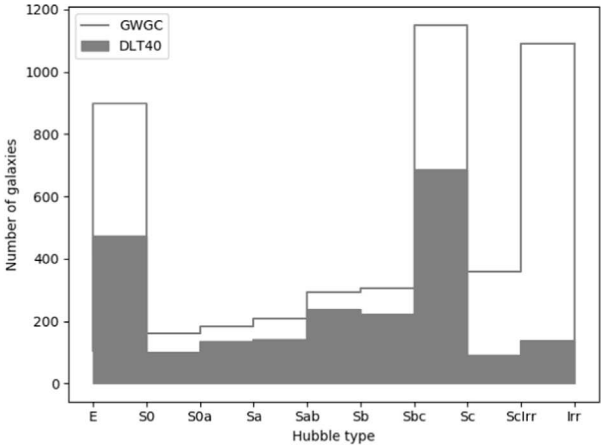

(b) The Hubble type distribution for DLT40 (shaded histogram) and GWGC galaxies (open histogram) within 40 Mpc.

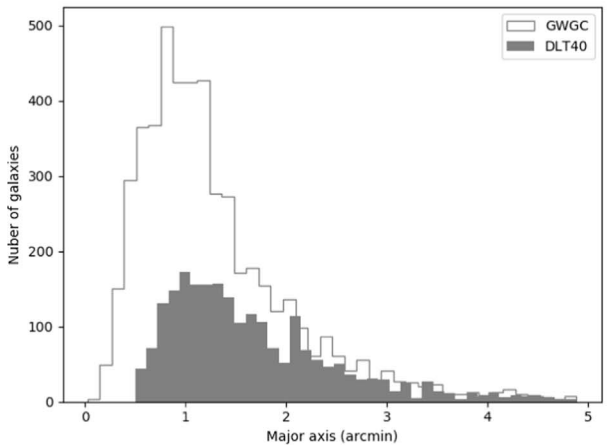

(c) The major axis distribution (in arcmin) for DLT40 (shaded histogram) and GWGC galaxies within 40 Mpc (open histogram).

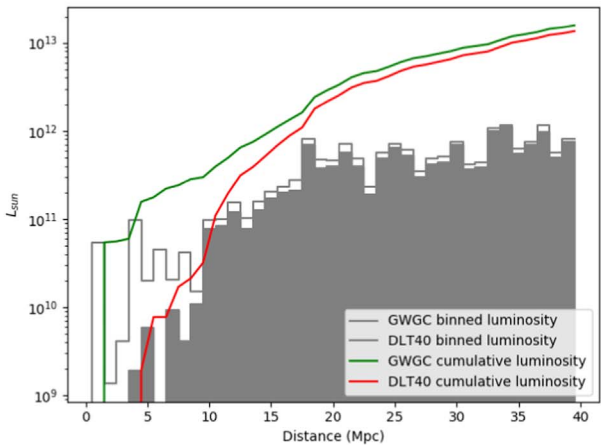

(d) The binned and integrated B band luminosity distribution for DLT40 and GWGC galaxies within 40 Mpc; note the binned points are difficult to distinguish on the scale of this plot.

Figure 1. Physical properties of the DLT40 galaxy sample compared with the GWGC (White et al. 2011).

the DLT40 team's follow-up observations (Valenti et al. 2017) and the limit to the kilonova rate using the DLT40 search (Yang et al. 2017). In Section 2 we provide an overview of the DLT40 supernova and transient program. A description of the DLT40 GW follow-up strategy in particular is described in Section 3. Next, in Section 4 we present the results of the DLT40 follow-up during O2. We discuss the DLT40 program's specific upgrades and plans for the imminent O3 observing run in Section 5. We end the paper with a brief discussion and summary (Section 6).

2. DLT40 Transient Search

The DLT40 survey is designed as a high-cadence supernova search. By targeting luminous galaxies within $D < 40$ Mpc, we aim to find ∼10 supernovae per year within ∼1 day of explosion. More details of the program are presented elsewhere (Yang et al. 2017; Tartaglia et al. 2018); we generally summarize them here. During the Advanced Detector O2 run, DLT40 used a PROMPT 0.4 m telescope (PROMPT5; Reichart et al. 2005) which has a field of view (FoV) of 10×10 arcmin^2 and is located at Cerro Tololo Inter-American Observatory (CTIO), part of the Skynet Robotic Telescope Network.[10] In a typical night, ∼400–500 galaxies are observed. The exposure time per field is 45 s, and the data are taken with no filter, yielding a typical limiting magnitude of $r \sim 19$ mag. The DLT40 galaxy sample is selected from the Gravitational Wave Galaxy Catalogue (GWGC; White et al. 2011), with further cuts made on recessional velocity ($V < 3000$ km s^{-1}, which corresponds to $D \lesssim 40$ Mpc), decl. (decl. $< +20°$), absolute magnitude ($M_B < -18$ mag), and Milky Way extinction ($A_V < 0.5$ mag). We maintained our original DLT40 galaxy sample even after the Galaxy List for the Advanced Detector Era[11] was made available because the completeness of the two catalogs is not significantly different within 40 Mpc (Dálya et al. 2018). The physical properties of the ∼2200 galaxies in the DLT40 sample are shown in Figure 1 in comparison to the whole GWGC sample within $D <$ 40 Mpc, selected without a luminosity cut.

[10] https://skynet.unc.edu/
[11] http://aquarius.elte.hu/glade

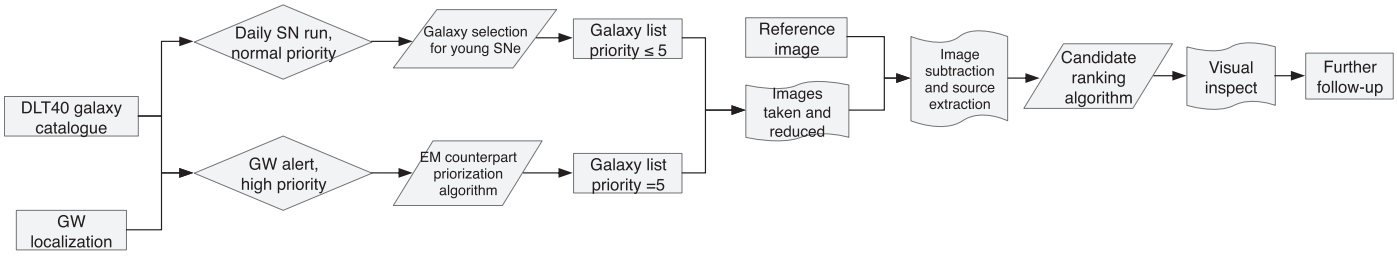

Figure 2. Work flowchart for the DLT40 survey.

The DLT40 survey is fully robotic, and a flowchart of operations is shown in Figure 2. A schedule is submitted automatically every afternoon before the Chilean sunset, and targets are given a priority between one and five. A score of five is the highest priority, and is reserved only for the most important targets such as the galaxies selected for GW follow-up. A score of four is assigned to galaxies that have been observed by the DLT40 survey over the last three days in order to maintain the program's cadence. A select few other galaxies are also given a native score of four—for instance, if they are within $D < 11$ Mpc, or if one PROMPT FoV can capture more than one DLT40 galaxy. A score of three is assigned to other DLT40 galaxies not selected with higher priority, and which have $M_B < -20$ mag, while a score of two is assigned to those galaxies with $M_B < -19$ mag. The remaining galaxies are given a score of one. The Skynet scheduler observes targets from west to east within a priority category so that all of the priority five galaxies are observed first (if visible), followed by the priority four galaxies, and so on. Galaxy priorities cannot be assigned in a "fine-grained" way beyond that described above, so in this sense all of the galaxies targeted for the DLT40 GW search were observed with an equally high priority, observed from west to east.

After an exposure is completed, the Skynet Robotic Telescope Network system automatically detrends the data (i.e., applies bias and flat field corrections), and determines an astrometric world coordinate system solution before the image is ingested by the DLT40 pipeline. From there, image subtraction is performed with respect to a high-quality template image using the publicly available `Hotpants` code (Becker 2015). `SExtractor`[12] (Bertin & Arnouts 1996) is then used to extract all sources in the difference images above a signal-to-noise threshold of five. The difference image source catalog typically includes a large number of spurious objects due to stochastic processes, small misalignments between the images, improper flux scalings, imperfect PSF matching between the template and target image, and cosmic rays. In order to filter out spurious candidates, a scoring algorithm was developed based on catalog parameters returned by `SExtractor`. This approach still required visual screening of a significant number of candidates, most of which are rejected. Recently, we have implemented a machine-learning algorithm for better filtering the spurious objects, which we discuss briefly along with our plans for the third observing run of the Advanced Detectors in Section 5.2. In order to manage our real-time data stream we use a `MySQL`[13] database and visually inspect SN candidates through web pages powered by the `Flask`[14] tool. After eyeballing, we secure immediate follow-up photometry or spectroscopy from collaborating facilities, most notably Las Cumbres Observatory, which itself is operated robotically (Brown et al. 2013).

The real-time and quick response of the DLT40 SN search make it ideal for rapidly evolving transients including the EM counterparts to GW sources. As such, DLT40 joined the global search effort during the Advanced Detector O2 run. We discuss our GW follow-up strategy in more detail in the next section.

3. GW Follow-up Strategy

The localization regions for GW events are still formidably large (especially compared to the DLT40 FoV), being of order $\lesssim$1000 deg^2 for two detector events and $\sim$10–100 deg^2 for three (e.g., Abbott et al. 2016d). Two complementary EM search strategies have been implemented by various groups thus far. The first involves direct tiling of the GW localization with wide-field telescopes in the search for counterparts (e.g., Abbott et al. 2016d; Kasliwal et al. 2016; Smartt et al. 2016; Soares-Santos et al. 2017; Doctor et al. 2019, among others), while the second relies on a targeted galaxy search focused on systems at a distance consistent with the GW signal that are also within the localization region (e.g., Gehrels et al. 2016). The DLT40 program followed the galaxy-targeted approach, although we relaxed any distance constraints whenever a GW event was beyond the nominal $\sim$40 Mpc horizon of the main SN search, as we describe below. The DLT40 PROMPT5 telescope's FoV ($10' \times 10'$) corresponds to 20 kpc (40 kpc) at a distances of 20 Mpc (40 Mpc), which encompasses >90% of expected merger-host offsets (Fong & Berger 2013), so each galaxy can be targeted with a single pointing.

3.1. Galaxy Prioritization

The DLT40 software suite ingests the GCN alerts employed during O2 for disseminating GW event information, and we download the `HEALPIX`localization map with distance constraints (see Singer & Price 2016; Singer et al. 2016, for further information on the generation of these maps). From this GW-based data, we prioritize galaxies in the DLT40 catalog given the position, relative probability within the localization map, and the galaxy's inferred mass. Again, we ignore any distance constraints from the GW signal in our galaxy prioritization algorithm (except for the nearby event GW170817). The target prioritization process is implemented as follows (see also Figure 3):

1. The DLT40 galaxy catalog is mapped with the `HEALPIX` tool, weighted by galaxy luminosity (we assume that the mass distribution follows the B-band luminosity), and smoothed with a Gaussian corresponding to each galaxy's reported radius. This yields a luminosity

[12] http://www.astromatic.net/software/sextractor
[13] https://www.mysql.com/
[14] http://flask.pocoo.org/

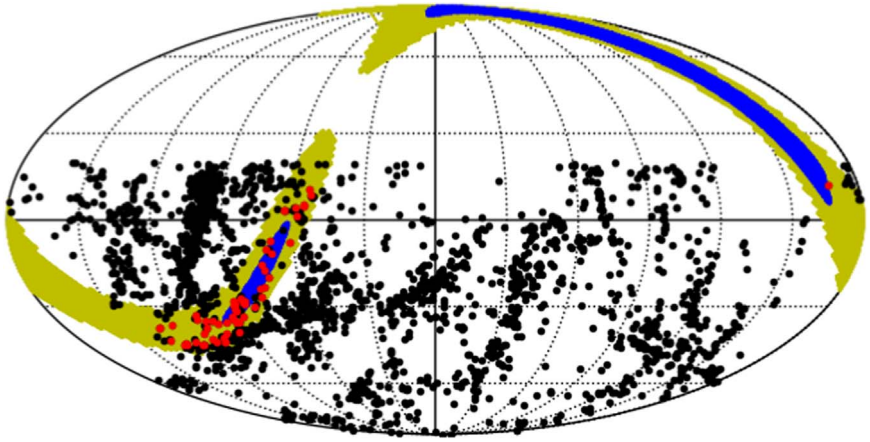

Figure 3. Illustration of the DLT40 galaxy ranking algorithm as applied to the LIGO trigger G275404. The full DLT40 galaxy sample is overlaid as black dots on the HEALPIX GW probability map; the blue and yellow regions present the 68% and 95% GW confidence regions, respectively. After normalization, a galaxy's score is defined as the accumulated pixel values inside the galaxy area, convolved with the GW probability map. The top ranked galaxies are selected for immediate follow-up and monitoring as described in Section 3. In the case of G275404, the red dots show the selected galaxies—not all DLT40 galaxies within the LIGO 95% confidence region were observed. We observed up to a cumulative score of 0.99 (50 galaxies) in the initial phase of our follow-up (see Section 4.1).

distribution map of DLT40 galaxies, $S_{\rm lum}$, which we normalize ($N_{\rm lum}$):

$$N_{\rm lum} = \frac{S_{\rm lum}}{\sum S_{\rm lum}}. \quad (1)$$

2. The GW probability map from LVC is already normalized as $S_{\rm gw}$.
3. We then take the product of the DLT40 galaxy map and the GW probability map,

$$C = S_{\rm gw} \times N_{\rm lum}. \quad (2)$$

4. For each DLT40 galaxy i, we sum over all pixels in C inside the galaxy radius, which yields our prioritization,

$$s_i = \sum_j C_{ij}, \quad (3)$$

where j is the HEALPIX pixel value inside the specific radius.

After the galaxy prioritization procedure, a cut on the number of monitored galaxies was made based on the level of interest in the GW trigger and practical observing considerations. For some GW sources with very large localization regions, we would also make cuts based directly on these maps —for instance, only selecting galaxy targets within the 80% credible region; see Section 4 for details on individual sources. We would select galaxies by cutting the ranked list at the top 50% - 99% of the normalized cumulative score, s, which would then be further reduced, because some galaxies in the list would be unobservable (i.e., below the horizon). For instance, if the GW trigger indicated the source was a local real (with a very low FAR) CBC, we would select galaxies up to a cumulative score of 99%, as shown in Figure 4. For those GW triggers that DLT40 followed up in O2, we observed between 18 and 114 galaxies per event, which corresponded to cumulative scores between 0.1 and 0.99. All the selected galaxies were set to priority 5 in the DLT40 scheduler.

As evidence of the efficacy of our galaxy prioritization algorithm, the highest priority galaxy for the BNS event GW170817 was NGC 4993, the true host galaxy of the counterpart (see Section 4.2 and Table 13 for further details). We discuss each individual GW event and our detailed follow-up from O2 further in Section 4.

In principle, we can adjust our galaxy prioritization to account for the GW-inferred distance (if given) and other detection efficiencies (similar to Fan et al. 2014; Arcavi et al. 2017b). For the LVC O2 run, we did not include the GW-inferred distance into our galaxy-targeting algorithm (which were only available for CBC triggers), but will do so for the DLT40 O3 campaign (Section 5.2).

3.2. Monitoring Timescale

The duration for which we monitor GW-related galaxies depends on the type of trigger. For burst-type GW events that are possibly related to core-collapse supernovae (with an optical timescale of ∼10–100 days), we adopt a monitoring period of three weeks. For BNS-type mergers, an r-process kilonova (Li & Paczyński 1998; Metzger et al. 2010; Kasen et al. 2013) and/or short gamma-ray burst (sGRB) afterglow emission is expected. Figure 5 shows different light-curve models for kilonovae and sGRB afterglow emission, scaled to a distance of 40 Mpc. As shown, DLT40 could detect transients predicted by most of the models out to this distance (the limiting magnitude of DLT40 is $r \sim 19$ mag, as measured by artificial star experiments, described in Yang et al. 2017). We thus conservatively monitored compact binary events for ∼2 weeks, well beyond the time we would generally expect to have a detection.

3.3. Summary

This galaxy prioritization process produces a list of galaxies that are sent automatically to the DLT40 scheduler. As discussed, these galaxies are observed at the highest priority, going from west to east on the sky, and are immediately ingested into our transient detection pipeline. All transient candidates were scored with our image feature-based algorithm and forwarded within minutes of data taking for visual inspection. If an interesting transient was found, a GCN was issued as soon as possible to facilitate follow-up observations; if no viable candidates were found, a summary GCN was usually posted in the following days to weeks.

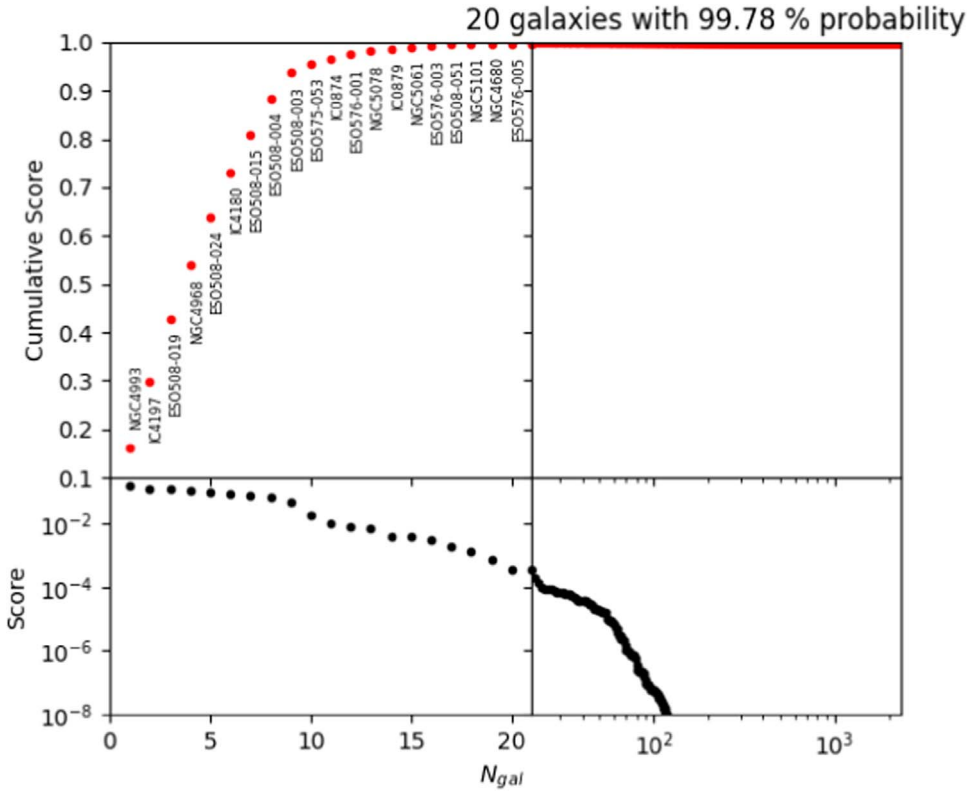

Figure 4. Cumulative score for DLT40 galaxies as prioritized for the NS–NS binary GW170817, using the algorithm described in Section 3. As shown, NGC 4993, the host of the kilonova DLT17ck/AT2017gfo, is ranked first. The 20 selected DLT40 galaxies cover 99.78% of the cumulative probability. More detailed information for each galaxy is presented in Table 13.

4. Search Results in O2

The LIGO O2 observing run ran from 2016 November 30 to 2017 August 25, with Virgo joining the network of GW detectors in early 2017 August. Fourteen GW alert triggers were issued (six of which turned out to be real events) by the LVC for follow-up to the EM community (The LIGO Scientific Collaboration & the Virgo Collaboration 2019), among which we followed the 10 triggers indicated in Table 1 (their localization is shown in Figure 6). Three of these 10 events that DLT40 followed up were ultimately found to be true GW events after further GW analysis (these are also marked in Table 1).

DLT40 pursued BBH events without prejudice during O2, even though these events may not have associated EM emission. GW horizon distances of BBH events are typically relatively large compared to the nominal reach of the DLT40 survey (focused on galaxies within 40 Mpc). For instance, the initial luminosity distance of G275697 estimated by the LVC has a mean value of 181 Mpc and standard deviation 55 Mpc (see Table 1; LIGO Scientific Collaboration & Virgo Collaboration 2017a). The cumulative probability within a 40 Mpc volume is only 1%. However, we activated our follow-up search for GW events outside the nominal DLT40 distance horizon for the following reasons:

1. As mentioned, during the LVC O2 run, the distance estimates of CBC are generally available, but are sometimes updated later or not reported in early circulars.
2. DLT40 is not dedicated to GW follow-up, so there is no conflict with our daily SN search—it does not harm us to search even if the probability of success is low.
3. The search could be implemented as a test run in preparation for events that DLT40 is more likely to find counterparts for (e.g., GW170817; Valenti et al. 2017).

For such BBH events with estimated GW distance beyond the reach of DLT40, we activated only the top 50% of galaxies scored by our ranking algorithm (see Section 3).

Here, we present our observations for the 10 DLT40-followed GW triggers, focusing first on the two events where our team identified optical transients. Unless otherwise noted, all dates listed are UTC. Detailed observational logs for each event are presented as a series of tables in the Appendix.

4.1. G275404

G275404 was identified as a marginal GW candidate by the two LIGO interferometers, Hanford (H1) and Livingston (L1) using the pyCBC analysis (Nitz et al. 2018) on 2017 February 25, 18:20:21.374 UTC (GPS time: 1172082639.374). The false alarm rate of 1.89×10^{-7} Hz corresponds to $\sim$1 in 0.17 yr. Following the initially released Bayestar localization map (Singer et al. 2016), the 50% (90%) credible region spanned about 460 (2100) deg^2. DLT40 responded rapidly (within an hour) to select 50 galaxies within the LVC error region, which were observed from 2017 February 26 to March 9. At 2017 March 8 22:30:50 UTC (11 days after the initial trigger), the LALInference localization map (Veitch et al. 2015) was issued by the LVC with a 50% (90%) credible region that increased to about 2000 (17,000) deg^2. Meanwhile, the LVC announced that the binary component masses were estimated to be consistent with a binary neutron star (BNS) or NS–BH binary (LIGO Scientific Collaboration & Virgo Collaboration 2017h).

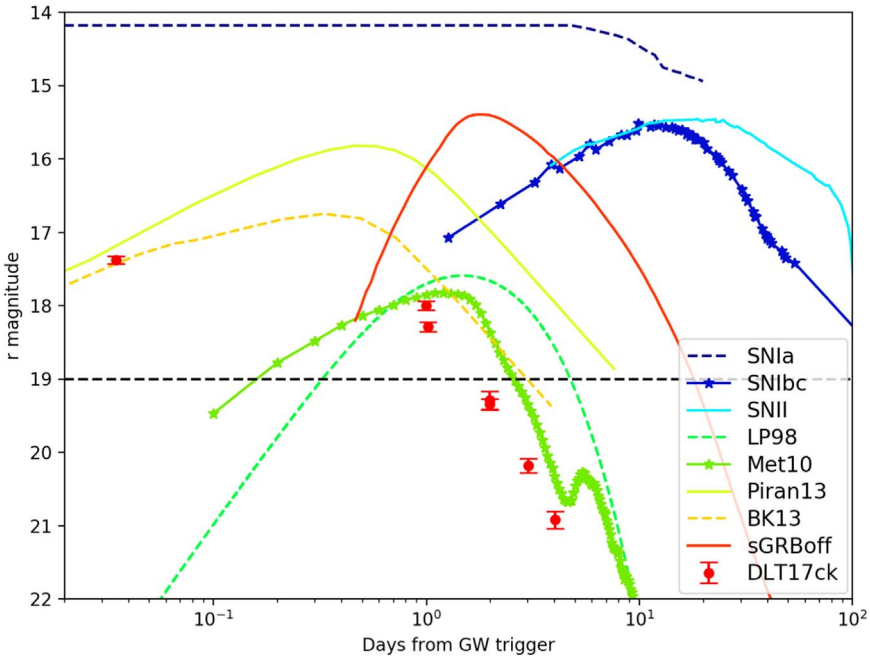

Figure 5. Several possible EM emission models of GW sources, scaled to a distance of 40 Mpc, are plotted against the 6 epochs of DLT17ck observations (red dots), as measured by the DLT40 survey (Valenti et al. 2017). Among these optical emission models, there are four kilonova models: LP98 (Li & Paczyński 1998), assuming a blackbody emission for an ejecta mass $10^{-2}\,M_{\odot}$, and outflow speed of $v = 0.1c$; Met10 (Metzger et al. 2010), assuming a radioactively powered emission with an ejecta mass $10^{-2}\,M_{\odot}$, and outflow speed of $v = 0.1c$, as well as iron-like opacities; BK13 (Barnes & Kasen 2013), assuming an ejected mass of $10^{-3}\,M_{\odot}$ and velocity of $0.1c$, along with lanthanide opacities; and Piran13 (Piran et al. 2013), assuming a BH–NS merger with NS $= 1.4\,M_{\odot}$, BH $= 10\,M_{\odot}$. We also include one sGRB off-axis model: sGRBoff (van Eerten & MacFadyen 2011), a simulated off-axis afterglow light curve assuming a short GRB with ejecta energy of $E_{\rm jet} = 10^{50}$ erg, interstellar matter density of $n = 10^{-3}\,{\rm cm}^{-3}$, jet half-opening angle of $\theta_{\rm jet} = 0.2$ radians, and an observed viewing angle of $\theta_{\rm obs} = 0.2$ radians. For comparison, we also show three SN light curves, including SN 2012cg (a SN Ia; Marion et al. 2016), SN2002ap (a SN Ib/c), and SN SN2013ej (a SN II; Yuan et al. 2016).

Starting on 2017 March 9 (until 2017 March 12) we re-prioritized our targeted galaxy list, and observed 84 galaxies using the updated GW localization map. The first 50 galaxies represent 3.9% of all galaxies in the Glade catalog within 40 Mpc and contain 12.7% of all B-band luminosity of those galaxies; the latter 84 galaxies represent 1.5% of all galaxies and contains 9.7% of all B band luminosity. The typical DLT40 limiting magnitude for these observations was 19.2 mag (open filter scaled to r band).

We found one SN Ia, SN2017cbv/DLT17u, in NGC 5643 (at a distance of $D \approx 12.3$ Mpc Sand et al. (2018) in the GW follow-up observations taken on 2017 March 8. Our follow-up observations of SN2017cbv/DLT17u with Las Cumbres Observatory telescopes show that SN2017cbv/DLT17u reached its maximum brightness ($B = 11.79$ mag) 17.7 days after discovery (Hosseinzadeh et al. 2017). Given the typical rise time of SNe Ia (18.98 ± 0.54 days; Firth et al. 2015), we deduced that SN2017cbv was discovered very close to the explosion epoch and we can thus exclude SN2017cbv from being related to the GW event, which occurred ∼2 weeks prior. Ultimately, further LVC analysis indicated that G275404 was not a trigger of interest (The LIGO Scientific Collaboration & the Virgo Collaboration 2019), confirming that SN 2017cbv was an unrelated transient.

4.2. GW170817/G298048

GW170817 (Abbott et al. 2017a, 2017b) was identified by the LIGO H1 detector at 2017 August 17 12:41:04 UTC (GPS time: 1187008882.4457), as a likely BNS merger event. The false alarm rate was 3.478×10^{-12} Hz, equivalent to ∼1 false alarm in 9100 yr. In addition, the GW candidate was found in coincidence with the *Fermi*/GBM trigger 524666471/170817529 (GRB 170817a; Goldstein et al. 2017), registered about 2 s later on 2017 August 17 12:41:06 UTC (GPS time: 1187008884.47). With further constraints from Virgo, the LVC joint sky area was reduced to 8.6 (33.6) deg^2 for the 50% (90%) credible regions, making it the best constrained event of the full O2 run. As shown in Figure 7, inside the 90% confidence region of GW170817 (33.6 deg^2), there were only 23 galaxies based on our DLT40 galaxy selection, and we decided to observe 20 of them (with 99% galaxy prioritization cut), together with the 31 most luminous galaxies in the GRB error-box region (Fermi GBM trigger). About ∼11 hr after the announcement of the GW trigger, at the beginning of the Chilean night, DLT40 reported the detection of DLT17ck at R.A. = 13:09:48.09 and decl. = −23:22:53.4.6, 5.37W, 8.60S arcsec from the center of NGC 4993 (Valenti et al. 2017; Yang et al. 2017h, 2017i, 2017j). Within one hour, we were one of the six optical groups that independently detected this optical transient, also named AT 2017 gfo and SSS17a (Abbott et al. 2017b; Arcavi et al. 2017a; Coulter et al. 2017; Lipunov et al. 2017; Soares-Santos et al. 2017; Tanvir et al. 2017; Valenti et al. 2017). It was soon established that DLT17ck was a GW-associated kilonova (Li & Paczyński 1998; Evans et al. 2017; Kasen et al. 2017; Metzger 2017; Pian et al. 2017; Villar et al. 2017). No other transients were found in the other surveyed galaxies that DLT40 followed in the GW170817 localization region. The DLT40 follow-up data obtained for DLT17ck are

Table 1
Summary Table of DLT40 Follow-up of LVC O2 Triggers

	LVC GW Estimations					DLT40 EM Observations			
GW/GRB trigger	Source type	FAR[a] (yr^{-1})	Localization[b] (deg^2)	D_{lum} (Mpc)	References[c]	N_{gal}	Obs_window (JD)	Detection[d] or r_{lim}	References[e]
GW170104[f] (G268556)	CBC	2	1600	⋯	a	18	2457759–2457766	⋯	⋯
G270580[f]	Burst	5	3100	⋯	b c	25	2457774–2457796	19.2	A
G274296	Burst	6	2100	⋯	d e	25	2457802–2457825	18.5	B
G275404	CBC	6	2100	280 ± 80	f	50	2457815–2457821	DLT17u	C
			17000	⋯	g	84	2457821–2457825	SN2017cbv (SN Ia)	
G275697	CBC	6	1800	181 ± 55	h	59	2457812–2457820	19.0	D
			3890	193 ± 61	i	114	2457820–2457825		
G277583	Burst	3	12140	⋯	j	55	2457826–2457847	19.5	E
G284239	Burst	4	3593	⋯	k	58	2457877–2457892	19.1	F
GW170608 (G288732)	CBC	2.6	860	320 ± 100	l	⋯	⋯	⋯	⋯
GW170809 (G296853)	CBC	0.25	1155	1000	m	⋯	⋯	⋯	⋯
GW170814 (G297595)	CBC	1/82800	97	550 ± 130	n	24	2457980–2457982	19.0	G
GW170817 (G298048)	CBC	1/9100	33.6	40 ± 8	o p	20	2457983–2457985	DLT17ck AT2017fgo (KN)	H I J
GRB 170817a					q	31			
G298389	Burst	6	799	⋯	r	⋯	⋯	⋯	⋯
GW170823 (G298936)	CBC	1/1800	2145	1387 ± 414	s	⋯	⋯	⋯	⋯
G299232	CBC	5.3	2040	339 ± 110	t	20	2457991–2458005	19	⋯

Notes. GW alert properties include the source type, the false alarm rate (FAR), the 90% confidence level sky localization area, and the luminosity distance. In the second column block, we report DLT40 observations, including the number of galaxies observed, their observation window, possible transients detected by DLT40 in that data set, and the reference GCNs. It should be mentioned that the GW estimates shown here are taken from the LVC preliminary and updated GCNs, the final GW estimation is shown in The LIGO Scientific Collaboration & the Virgo Collaboration (2019).

[a] The "FAR" column is the estimated false alarm rate per year, while the LVC threshold is 1 per month or 12 per year. If the FAR is less than 12, an alert would be issued.

[b] The "localization" column is the uncertainty area of GW triggers in the 90% confidence level.

[c] a. LIGO Scientific Collaboration & Virgo Collaboration (2017b), b. LIGO Scientific Collaboration & Virgo Collaboration (2017c), c. LIGO Scientific Collaboration & Virgo Collaboration (2017d), d. LIGO Scientific Collaboration & Virgo Collaboration (2017e), e. LIGO Scientific Collaboration & Virgo Collaboration (2017f), f. LIGO Scientific Collaboration & Virgo Collaboration (2017g), g. LIGO Scientific Collaboration & Virgo Collaboration (2017h), h. LIGO Scientific Collaboration & Virgo Collaboration (2017a), i. LIGO Scientific Collaboration & Virgo Collaboration (2017i), j. LIGO Scientific Collaboration & Virgo Collaboration (2017j), k. LIGO Scientific Collaboration & Virgo Collaboration (2017k), l. LIGO Scientific Collaboration & Virgo Collaboration (2017l), m. LIGO Scientific Collaboration & Virgo Collaboration (2017m), n. LIGO Scientific Collaboration & Virgo Collaboration (2017n), o. LIGO Scientific Collaboration & Virgo Collaboration (2017o), p. LIGO Scientific Collaboration & Virgo Collaboration (2017p), q. LIGO Scientific Collaboration & Virgo Collaboration (2017q), r. LIGO Scientific Collaboration & Virgo Collaboration (2017r), s. LIGO Scientific Collaboration & Virgo Collaboration (2017s), t. LIGO Scientific Collaboration & Virgo Collaboration (2017t).

[d] We report the typical DLT40 limiting magnitude (r band) for the observation set in the "Detection" column.

[e] A. Yang et al. (2017a), B. Yang et al. (2017b), C. Yang et al. (2017c), D. Yang et al. (2017d), E. Yang et al. (2017e), F. Yang et al. (2017f), G. Yang et al. (2017g), H. Yang et al. (2017h), I. Yang et al. (2017i), J. Yang et al. (2017j).

[f] For GW170104 (G268556) and G270580 we only observed DLT40 galaxies out to 20 Mpc within the LVC localization as a test run.

described in Valenti et al. (2017). Yang et al. (2017) further used the observed light curve of DLT17ck to constrain the rate of BNS mergers to be less than 0.50 SNuB[15] and we concluded that DLT40 would need to operate for ∼18.4 yr in order to discover a kilonova without a GW trigger.

4.3. Other GW Triggers

GW170104/G268556 (Abbott et al. 2017c; LIGO Scientific Collaboration & Virgo Collaboration 2017b) was identified by L1 and H1 at 2017 January 4 10:11:58.599 UTC (GPS time: 1167559936.599). GW170104 was a BBH event with a low false alarm rate, 6.1×10^{-8} Hz (about one in 6 months). This GW event was the first identified LVC trigger in the O2 run, and the first GW event followed by DLT40. The initial announcement of GW170104/G268556 did not include a distance estimate. For this first event, we decided to test our galaxy ranking algorithm and other infrastructure as a dry run, and not report our findings via a GCN. We monitored 18 galaxies within 20 Mpc for ∼1 week within the 90% GW localization region, and no optical counterpart candidates were found.

G270580 (LIGO Scientific Collaboration & Virgo Collaboration 2017c, 2017d) was identified by L1 and H1 at 2017 January 20 12:30:59.350 UTC (GPS time: 1168950677.350). The false alarm rate was 1.6×10^{-7} Hz (about one in 2.4 months). The 50% credible region spanned about 600 deg^2 and the 90% region spanned about 3100 deg^2. We observed 25 galaxies from the DLT40 catalog within the 99% credible

[15] SNuB = 1 SN per 100 yr per $10^{10} L_{B_\odot}$.

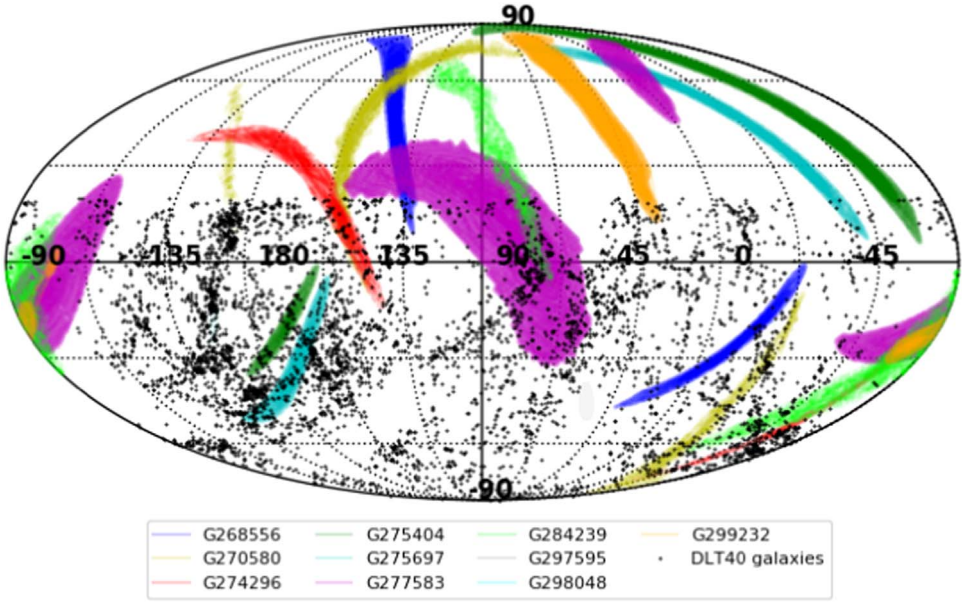

Figure 6. The DLT40 galaxy sample super-imposed on the 68% confidence contours of the ten LVC triggers followed by DLT40 during O2. See Section 4 and Table 1 for further details.

region, again within a distance of 20 Mpc, from 2017 January 23 onward, for three weeks. No interesting transients were identified down to a typical limiting magnitude of 19.2 mag in the r band (Yang et al. 2017a). This GW event was ultimately retracted by the LVC.

G274296 (LIGO Scientific Collaboration & Virgo Collaboration 2017e, 2017f) was identified as a burst candidate by H1 and L1 at 2017 February 17 06:05:55.050 UTC (GPS time:1171346771.050), with false alarm rate 1.7×10^{-7} Hz, or about 1 in 2 months. We observed 25 galaxies from our DLT40 galaxy catalog (out to the full DLT40 $D = 40$ Mpc search volume) within the 80.0% credible region of the trigger localization region. We began observing these galaxies on 2017 February 17 and monitored them for 3 weeks after the GW trigger. No interesting transients were identified down to an average limiting magnitude of 18.5 (Yang et al. 2017b). The LVC ultimately classified this GW trigger as of no further interest.

G275697 (LIGO Scientific Collaboration & Virgo Collaboration 2017a, 2017i) was identified as a marginal candidate by L1 and H1 at 2017 February 27 18:57:31.375 UTC (GPS time: 1172257069.375), with a false alarm rate of 1.43×10^{-7} Hz or about 1 in 2 months. Based on a preliminary analysis, the LVC reported that the less massive component in the binary had a mass $<3\,M_{\rm Sun}$ and that there was a 100% chance that the system ejected enough neutron-rich material to power an electromagnetic transient. The 50% credible region spanned about 480 deg^2 and the 90% region about 1800 deg^2. The luminosity distance was estimated to be 181 ± 55 Mpc. We observed 59 galaxies from 2017 February 27 to March 7. After an update of the LVC localization map, we updated the galaxy sample and observed 114 galaxies from 2017 March 7 to 12. No interesting transients were identified down to a limiting magnitude of ≈19.0 (Yang et al. 2017d). The final analysis of the LVC indicated that G275697 was not a trigger of interest.

G277583 (LIGO Scientific Collaboration & Virgo Collaboration 2017j) was identified as a burst candidate by L1 and H1 at 2017 March 13 22:40:09.593 UTC (GPS time:1173480027.593). Its false alarm rate was 8.4×10^{-8} Hz (1 in 4 months). We observed 55 galaxies within the 80.0% credible region, beginning on 2017 March 13 and continuing for 2 weeks after the GW trigger. No interesting transients were identified down to a limiting magnitude of 19.5 mag (Yang et al. 2017e). The final analysis of the LVC indicated that G277583 was not a trigger of interest.

G284239 (LIGO Scientific Collaboration & Virgo Collaboration 2017k) was identified by L1 and H1 at 2017 May 02 22:26:07.910 UTC (GPS time: 1177799185.910). G284239 was a low-significance short-duration burst candidate whose false alarm rate was 1.26×10^{-7} Hz (4 per year). The 50% confidence region covered 1029 deg^2 and the 90% confidence region covered 3593 deg^2. We observed 58 galaxies within the 95% credible region of the localization for a duration of two weeks starting on 2017 May 2 (Yang et al. 2017f). No interesting transients were identified down to a limiting magnitude of $r \sim 19$ mag. The LVC determined that this event was of no further interest.

G297595/GW170814 (LIGO Scientific Collaboration & Virgo Collaboration 2017n) was the first GW event detected by both LIGO detectors (H1, L1) and the Virgo (V1) detector (Abbott et al. 2017d) at 2017 August 14 10:30:43 UTC (GPS time: 1186741861.5268). The Virgo detection helped to decrease the 50% (90%) localization region from 333 (1158) deg^2 to 22 (97) deg^2. GW170814 had a very low false alarm rate of 3.83×10^{-13} Hz, equivalent to ∼1 per 82,800 yr. The LVC reported that the event was a BBH merger at $\sim 550 \pm 130$ Mpc. Despite the lack of an expected optical counterpart and the large distance, we triggered follow up partly because of the small localization region. We monitored 24 galaxies within the LVC error region with an average limiting magnitude of 19.0 mag (Yang et al. 2017g). No obvious optical counterparts were detected. All selected galaxies from this trigger were reset to normal priority on 2017 August 17 in order to aggressively pursue the next trigger, GW170817.

G299232 (LIGO Scientific Collaboration & Virgo Collaboration 2017t) was identified by L1 and H1 at 2017 August 25 13:13:31 UTC (GPS time: 1187702035.9831). G299232 was a low-significance candidate with a false alarm rate of 1.68×10^{-7} Hz (about 5.3 per year). The 50% credible

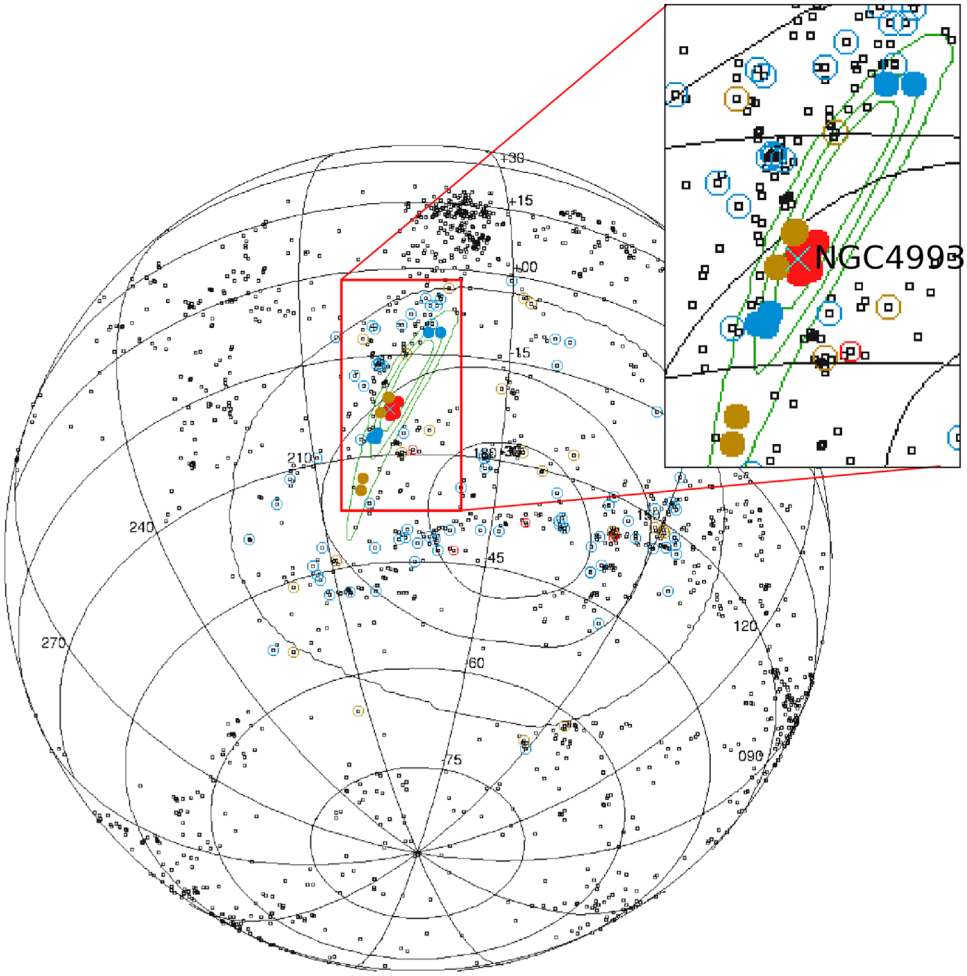

Figure 7. Localization region (contours) and the matched galaxies (circles) for GW170817/G298048 (solid circles) and GRB 170817a (hollow circles). The contours indicate 50%, 90%, and 99% confidence bounds, while the GW trigger is shown in green and the GRB trigger is shown in black. The colors of the circles denote the priority of the galaxies (high priority in red, normal priority in yellow, and low priority in blue). All the DLT40 galaxy samples are shown as black dots. After ranking, we decided to follow all 20 GW galaxies (9 high + 5 normal + 6 low) and the top 31 GRB galaxies (5 high + 26 normal).

region spanned about 450 deg^2 and the 90% region spanned about 2040 deg^2. We selected and observed 41 galaxies within 95.0% of the trigger localization region from 2017 August 25 to 2017 September 8. No obvious transient was found, and the LVC concluded that this event was of no further interest.

5. Future Prospects

In this section, we describe the DLT40 project's follow-up plans for the upcoming LVC O3 run based on some simple simulations of GW events, and the performance of DLT40.

5.1. DLT40 EM Counterpart Potential

To evaluate DLT40's potential impact for O3, we made use of the artificial star tests described in Yang et al. (2017), which provide point source detection efficiencies as a function of image zero-point and seeing. Using these artificial star tests in conjunction with the real light curve of AT2017gfo/DLT17ck and the EM counterpart models shown in Figure 5, we calculate the limiting distance out to which the DLT40 program can detect each of these transients, as shown in Figure 8. Kilonovae with light curves similar to AT2017gfo/DLT17ck can be detected out to $D \approx 80$ Mpc, while other kilonova light-curve models have similar limiting distances. For O3, the expected distance sensitivity of advanced LIGO to BNS mergers will be $D \approx 120$–170 Mpc, while for Virgo it will be $D \approx 65$–85 Mpc (Abbott et al. 2016e, 2018).[16] If we assume that all kilonovae are as bright as AT2018gfo/DLT17ck and neglect that any potential galaxy catalog is incomplete, the current DLT40 observing strategy could detect all kilonovae in the Virgo volume during the O3 run. In the end, rather than going out to the full ≈80 Mpc distance horizon of Virgo for O3, we chose a distance at the lower end of their expected sensitivity ($D \approx 65$ Mpc), which was more practical for the purposes of gathering template images of all the necessary galaxy fields.

5.2. DLT40 Plans for O3

The DLT40 survey is continually upgrading its hardware and software, and we have been making special plans for the LVC O3 run; we summarize these improvements here.

1. As shown in Section 5.1, the depth and cadence of DLT40 is suitable for finding typical kilonovae out to the horizon of the Virgo detector during O3. We are thus gathering template images of galaxies out to $D \approx 65$ Mpc

[16] These distance ranges are the volume- and orientation-averaged distance at which a CBC of a given mass yields a matched filter signal-to-noise ratio (SNR) of 8 in a single detector.

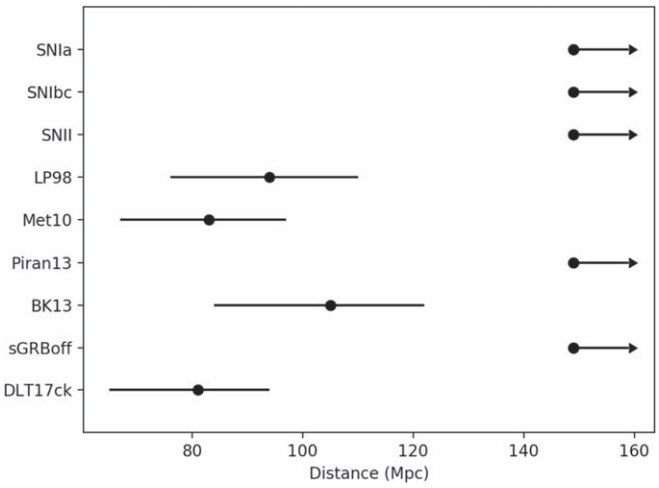

Figure 8. The DLT40 limiting distance for different BNS EM emission models (details described in Figure 5), and the observational data of DLT17ck, are estimated. The computational recipe is as follows: (1) detection efficiency (DE) for a single epoch/point: by setting up a series of artificial star experiments, we obtain the DE plots, which show the relations between the DLT40 DE, with magnitude, for a specific field (Yang et al. 2017); (2) DE for an epochs/sampling light curve: for a specific light curve (EM models or observations in absolute magnitudes), by executing step 1 for a sample of epochs (we decide the sample points by comparing the burst time of GW170817, with our DLT40 observing epochs toward NGC 4993.), we obtain DE_j for each epoch, while the overall DE is derived as $DE = 1 - \Sigma_j(1 - \mathrm{DE}_j)$; (3) limiting distance estimation: we scaled each light curve to a distance of D_i, and obtain $\mathrm{DE}_{D=D_i}$ at different distances. The limiting distance is then defined as the distance where $\mathrm{DE}_{D=D_i}$ is 50%.

(drawn from the GWGC, with decl. $< +20°$, $M_B < -18$ mag and $A_V < 0.5$ mag, as with the rest of the standard DLT40 search), in preparation for following up merger events with a neutron star in O3.

2. The DLT40 team has recently added a second identical telescope to its SN search, located at Meckering Observatory in western Australia. This telescope will be utilized on an equal footing to the original DLT40 telescope at CTIO, and makes our GW counterpart search more robust to weather and instrument problems. It also decreases our response time to any given event, given our distributed longitudinal coverage. DLT40 is also in the process of incorporating a third telescope in Alberta, Canada, which will likely be operational near the currently planned start of O3 (2019 April). This telescope will provide northern hemisphere coverage for the DLT40 EM counterpart search.
3. Several recent improvements have been made to the overall DLT40 pipeline. Chief among them has been the adoption of a pixel-based, random forest, machine-learning algorithm used for scoring incoming SN candidates in real time (based on the algorithm used by the Pan-STARRS1 survey; Wright et al. 2015). This algorithm has drastically shrunken the number of transient candidates that must be inspected in a given night's worth of data ($\sim$10 s instead of $\sim$1000 s). In addition, very strong transient candidates with high machine-learning scores trigger automated email alerts to the DLT40 team, which can respond with follow-up imaging on either DLT40 telescope within minutes.
4. The DLT40 GW follow-up code will respond autonomously to incoming LVC alerts, inserting the appropriate galaxy targets into the DLT40 scheduler at high priority in real time. It will also alert the team if a counterpart candidate appears in a selected field (see point 3). DLT40 will respond to all burst alerts in O3 (which will not have distance information), as well as all CBC alerts that have a cumulative probability of $>10\%$ of being within $D < 65$ Mpc (we intend to follow all nearby CBC alerts. In case the trigger rate is relatively high in O3, e.g., several sources within one week, we would manually evaluate them with the false alarm rate and the probability of which contains a neutron star).

6. Summary

We have presented the GW follow-up strategy and results for the DLT40 survey during the O2 observing run of Advanced LIGO and Virgo. DLT40 employed a galaxy-targeted search that combined the GW localization region and the galaxy catalog employed by the DLT40 SN search to prioritize targets for follow-up. This strategy bore fruit for GW170817, the first detected BNS merger, as DLT40 co-discovered the associated kilonova AT2017gfo/SSS17a/DLT17ck (Valenti et al. 2017). In all, we present follow-up observations of 10 out of the 16 O2 GW triggers. Of these 10, 3 events were ultimately verified as *bona fide* GW events.

Finally, in Section 5 we discussed the DLT40 team's follow-up plans for the upcoming O3 detector run. Two additional, identical telescopes will be added in Australia and Canada, providing longitudinal and northern hemisphere coverage. Automated response to new GW events with allow for immediate scheduling of high-priority galaxy fields on one of DLT40's search telescopes, and a new machine-learning algorithm will cleanly identify new transient events and notify the team within minutes if a strong optical counterpart candidate is found. Furthermore, artificial star experiments indicate that DLT40 will be sensitive to kilonovae out to the neutron star merger horizon of Virgo during O3, and we will respond to any appropriate event out to $D \approx 65$ Mpc. Small robotic telescope systems, coupled with smart software, will continue to have an out-sized impact on multi-messenger astrophysics in the years ahead.

S.Y. would like to thank Marica Branchesi and He Gao for helpful discussions and comments. S.Y. acknowledges from the China Scholarship Council #201506040044, and the support by the PRIN-INAF 2016 with the project "Toward the SKA and CTA era: discovery, localization, and physics of transient source." Research by D.J.S. is supported by NSF grants AST-1821967, 1821987, 1813708, and 1813466. Research by S.V. is supported by NSF grant AST-1813176. The DLT40 webpage structures were developed at the Aspen Center for Physics, which is supported by National Science Foundation grant PHY-1066293. A.C. acknowledges support from the NSF award #1455090 "CAREER: Radio and gravitational-wave emission from the largest explosions since the Big Bang."

Software: Hotpants (Becker 2015), SExtractor (Bertin & Arnouts 1996), Healpix (Górski et al. 2005), Astropy (Astropy Collaboration et al. 2018).

Appendix
DLT40 GW Follow-up Observing Logs for the LVC O2 Run

Tables 2–14 present the DLT40 galaxies that were selected, activated and followed by us during the second observing run of the LVC. In each of the presented galaxy lists, we display target galaxy information (from the GWGC; White et al. 2011), including the galaxy name, equatorial coordinates, luminosity distance, and absolute magnitude in the *B* and *K* bands. We also include details of the observations, including the observing window, and the score estimated by our DLT40 galaxy prioritization algorithm. This information was also presented in the DLT40 team's O2 GCNs.

Table 2
Galaxies Observed after Trigger GW170104/G268556

Name (1)	R.A.(J2000) (2)	Decl.(J2000) (3)	Dist(Mpc) (4)	*B*(mag) (5)	*K*(mag) (6)	Obs_Window(JD) (7)	Score (8)
NGC 7507	348.03	−28.54	25.00	−20.77	−24.70	2457759.33–2457766.29	2.033×10^{-1}
NGC 7755	356.97	−30.52	27.92	−20.63	−23.26	2457759.33–2457766.29	6.838×10^{-2}
NGC 1291	49.33	−41.11	10.38	−20.66	−24.42	2457759.33–2457766.29	1.823×10^{-2}
NGC 1448	56.13	−44.64	15.35	−20.30	−23.27	2457759.33–2457766.29	1.013×10^{-2}
NGC 1365	53.40	−36.14	17.95	−21.39	−24.90	2457759.33–2457766.29	8.132×10^{-3}
NGC 2263	99.62	−24.85	32.36	−20.75	−23.41	2457759.33–2457766.29	5.403×10^{-3}
NGC 1411	54.69	−44.10	19.77	−19.78	−23.33	2457759.33–2457766.29	5.345×10^{-3}
ESO 557-009	99.68	−20.29	32.08	−20.52	−21.91	2457759.33–2457766.29	4.550×10^{-3}
IC 0438	88.25	−17.88	36.64	−20.33	−23.12	2457759.33–2457766.29	4.188×10^{-3}
NGC 7713A	354.28	−37.71	36.67	−20.15	−22.27	2457759.33–2457766.29	3.945×10^{-3}
NGC 2217	95.42	−27.23	20.80	−20.31	−24.50	2457759.33–2457766.29	3.910×10^{-3}
NGC 2350	108.30	12.27	28.84	−20.00	−23.04	2457759.33–2457766.29	3.750×10^{-3}
NGC 2089	86.96	−17.60	38.11	−20.33	−24.09	2457759.33–2457766.29	3.740×10^{-3}
IC 2143	86.72	−18.73	38.02	−20.12	−23.20	2457759.33–2457766.29	3.546×10^{-3}
PGC 018581	92.78	−15.49	24.21	−19.87	−21.74	2457759.33–2457766.29	2.972×10^{-3}
PGC 085930	99.80	−1.51	36.83	−20.43	−23.90	2457759.33–2457766.29	2.850×10^{-3}
NGC 7371	341.52	−11.00	29.92	−19.74	−23.14	2457759.33–2457766.29	2.437×10^{-3}
NGC 2377	111.24	−9.66	29.92	−20.17	−23.37	2457759.33–2457766.29	2.330×10^{-3}

Note. The table columns provide the galaxy name, coordinates, distance, *B*- and *K*-band magnitudes, observing window, and the score from our ranking algorithm. The cumulative score is 0.357.

Table 3
Galaxies Observed after Trigger G270580

Name (1)	R.A.(J2000) (2)	Decl.(J2000) (3)	Dist(Mpc) (4)	*B*(mag) (5)	*K*(mag) (6)	Obs_Window(JD) (7)	Score (8)
NGC 4419	186.74	15.05	13.49	−19.24	−22.91	2457991.48–2458005.21	2.703×10^{-2}
NGC 4216	183.98	13.15	14.13	−20.58	−24.23	2457991.48–2458005.21	1.633×10^{-2}
IC 5201	335.24	−46.03	9.20	−18.78	−19.65	2457991.48–2458005.21	9.84×10^{-3}
NGC 4571	189.23	14.22	14.93	−19.12	−22.35	2457991.48–2458005.21	9.603×10^{-3}
NGC 4498	187.91	16.85	14.06	−18.54	−21.08	2457991.48–2458005.21	9.24×10^{-3}
NGC 4192	183.45	14.90	13.61	−20.62	−23.78	2457991.48–2458005.21	5.19×10^{-3}
NGC 4178	183.19	10.87	14.00	−19.37	−21.16	2457991.48–2458005.21	5.118×10^{-3}
NGC 1546	63.65	−56.06	13.87	−18.21	−22.66	2457991.48–2458005.21	4.41×10^{-3}
NGC 0253	11.89	−25.29	3.94	−20.06	−24.21	2457991.48–2458005.21	3.267×10^{-3}
NGC 1559	64.40	−62.78	12.59	−19.85	−22.48	2457991.48–2458005.21	2.509×10^{-3}
NGC 1566	65.00	−54.94	6.55	−18.89	−22.20	2457991.48–2458005.21	1.830×10^{-3}
NGC 2640	129.35	−55.12	12.71	−20.17	−23.81	2457991.48–2458005.21	1.770×10^{-3}
NGC 1947	81.70	−63.76	13.87	−19.01	−23.21	2457991.48–2458005.21	1.323×10^{-3}
NGC 4123	182.05	2.88	14.86	−19.09	−22.07	2457991.48–2458005.21	1.072×10^{-3}
NGC 1617	67.92	−54.60	13.87	−19.79	−23.63	2457991.48–2458005.21	1.017×10^{-3}
NGC 1602	66.98	−55.06	13.69	−18.48	−18.66	2457991.48–2458005.21	9.102×10^{-4}
IC 2056	64.10	−60.21	15.00	−18.48	−21.73	2457991.48–2458005.21	8.838×10^{-4}
NGC 1796	75.68	−61.14	15.00	−18.28	−21.18	2457991.48–2458005.21	7.911×10^{-4}
NGC 7090	324.12	−54.56	6.28	−18.56	−20.83	2457991.48–2458005.21	6.363×10^{-4}
ESO 097-013	213.29	−65.34	4.21	−19.03	−23.14	2457991.48–2458005.21	6.333×10^{-4}
NGC 1249	47.51	−53.34	14.19	−19.16	−21.41	2457991.48–2458005.21	5.976×10^{-4}
NGC 3521	166.45	−0.04	11.22	−20.85	−24.47	2457991.48–2458005.21	5.433×10^{-4}
ESO 494-026	121.55	−27.53	14.15	−19.86	−22.88	2457991.48–2458005.21	2.601×10^{-4}
IC 1954	52.88	−51.90	13.68	−18.98	−21.93	2457991.48–2458005.21	2.021×10^{-4}
NGC 1313	49.56	−66.50	4.07	−18.79	−20.48	2457991.48–2458005.21	1.706×10^{-4}
ESO 054-021	57.46	−71.63	13.87	−18.85	−20.36	2457991.48–2458005.21	1.467×10^{-4}
NGC 7814	0.81	16.15	13.18	−19.68	−23.52	2457991.48–2458005.21	1.438×10^{-4}
NGC 2784	138.08	−24.17	9.82	−19.42	−23.64	2457991.48–2458005.21	9.909×10^{-5}

Table 3
(Continued)

Name (1)	R.A.(J2000) (2)	Decl.(J2000) (3)	Dist(Mpc) (4)	*B*(mag) (5)	*K*(mag) (6)	Obs_Window(JD) (7)	Score (8)
NGC 2835	139.47	−22.35	8.05	−19.03	−21.61	2457991.48–2458005.21	8.748×10^{-5}
NGC 0014	2.19	15.82	13.87	−18.61	−20.29	2457991.48–2458005.21	6.519×10^{-5}
NGC 0428	18.23	0.98	14.79	−19.12	−21.46	2457991.48–2458005.21	5.913×10^{-5}
NGC 2283	101.47	−18.21	9.86	−18.17	−19.85	2457991.48–2458005.21	3.786×10^{-5}
PGC 018855	95.23	−8.50	11.22	−18.39	−21.94	2457991.48–2458005.21	3.753×10^{-5}

Note. The table columns provide the galaxy name, coordinates, distance, *B*- and *K*-band magnitudes, observing window, and the score from our ranking algorithm. The cumulative score is 0.106.

Table 4
Galaxies Observed after Trigger G274296

Name (1)	R.A.(J2000) (2)	Decl.(J2000) (3)	Dist(Mpc) (4)	*B*(mag) (5)	*K*(mag) (6)	Obs_Window(JD) (7)	Score (8)
IC 4837A	288.82	−54.13	33.42	−21.15	−24.47	2457802.38–2457825.37	4.803×10^{-2}
IC 4837	288.81	−54.67	33.42	−20.72	−20.38	2457802.38–2457825.37	3.770×10^{-2}
IC 4839	288.89	−54.63	35.11	−20.02	−23.48	2457802.38–2457825.37	3.770×10^{-2}
NGC 3041	148.28	16.68	23.77	−19.86	−23.14	2457802.38–2457825.37	3.738×10^{-2}
NGC 6788	291.71	−54.95	34.56	−21.09	−24.17	2457802.38–2457825.37	3.607×10^{-2}
NGC 2698	133.90	−3.18	24.94	−18.89	−23.14	2457802.38–2457825.37	3.437×10^{-2}
NGC 2708	134.03	−3.36	26.55	−19.15	−23.24	2457802.38–2457825.37	3.437×10^{-2}
NGC 2697	133.75	−2.99	24.17	−18.59	−22.02	2457802.38–2457825.37	3.041×10^{-2}
NGC 2695	133.61	−3.07	32.36	−19.76	−23.70	2457802.38–2457825.37	3.041×10^{-2}
NGC 2706	134.05	−2.56	21.88	−18.48	−22.18	2457802.38–2457825.37	2.778×10^{-2}
NGC 2775	137.58	7.04	17.30	−20.17	−24.15	2457802.38–2457825.37	2.725×10^{-2}
NGC 2919	143.70	10.28	34.67	−19.54	−22.65	2457802.38–2457825.37	2.151×10^{-2}
NGC 2722	134.69	−3.71	38.02	−19.68	−22.49	2457802.38–2457825.37	2.111×10^{-2}
IC 0540	142.54	7.90	28.64	−18.75	−21.77	2457802.38–2457825.37	2.010×10^{-2}
NGC 2690	133.16	−2.60	21.04	−18.61	−21.97	2457802.38–2457825.37	1.944×10^{-2}
NGC 2906	143.03	8.44	29.92	−19.28	−23.27	2457802.38–2457825.37	1.905×10^{-2}
NGC 2894	142.38	7.72	30.49	−19.75	−23.31	2457802.38–2457825.37	1.814×10^{-2}
NGC 6810	295.89	−58.66	23.12	−20.42	−24.14	2457802.38–2457825.37	1.742×10^{-2}
NGC 3226	155.86	19.90	23.55	−19.59	−23.29	2457802.38–2457825.37	1.741×10^{-2}
UGC 05467	152.05	18.71	39.71	−18.96	−22.15	2457802.38–2457825.37	1.220×10^{-2}
IC 4821	287.38	−55.02	25.00	−18.98	−21.61	2457802.38–2457825.37	1.144×10^{-2}
IC 2367	126.04	−18.78	29.18	−20.71	−23.89	2457802.38–2457825.37	1.141×10^{-2}
IC 4797	284.12	−54.31	28.05	−20.23	−24.17	2457802.38–2457825.37	1.103×10^{-2}
PGC 024778	132.25	−7.83	38.02	−19.75	−22.33	2457802.38–2457825.37	9.475×10^{-3}
NGC 6920	310.99	−80.00	32.99	−20.52	−24.22	2457802.38–2457825.37	9.363×10^{-3}
UGC 05403	150.65	19.18	33.42	−18.48	−22.28	2457802.38–2457825.37	9.153×10^{-3}
ESO 231-017	286.19	−47.85	35.14	−19.62	−23.20	2457802.38–2457825.37	8.543×10^{-3}
NGC 6844	300.71	−65.23	36.98	−19.60	−23.47	2457802.38–2457825.37	7.537×10^{-3}
IC 4889	296.31	−54.34	29.24	−20.33	−24.22	2457802.38–2457825.37	7.368×10^{-3}
PGC 023658	126.49	−11.78	38.93	−19.84	−21.71	2457802.38–2457825.37	7.059×10^{-3}
NGC 3020	147.53	12.81	21.88	−19.20	−21.02	2457802.38–2457825.37	6.063×10^{-3}
NGC 3024	147.61	12.77	25.35	−18.92	−20.84	2457802.38–2457825.37	6.063×10^{-3}
PGC 023723	126.89	−12.76	34.61	−19.08	−21.69	2457802.38–2457825.37	5.956×10^{-3}
UGC 04684	134.17	0.38	35.67	−18.54	−20.52	2457802.38–2457825.37	5.682×10^{-3}
IC 4871	293.93	−57.52	22.59	−18.80	−20.88	2457802.38–2457825.37	5.112×10^{-3}
IC 4901	298.60	−58.71	17.86	−19.61	−22.41	2457802.38–2457825.37	4.946×10^{-3}
IC 4817	286.55	−56.16	33.42	−18.96	−21.27	2457802.38–2457825.37	4.438×10^{-3}
IC 5071	315.33	−72.64	30.90	−19.65	−22.94	2457802.38–2457825.37	4.270×10^{-3}
IC 5026	312.12	−78.07	32.36	−19.16	−20.55	2457802.38–2457825.37	3.636×10^{-3}
NGC 2612	128.46	−13.17	21.67	−18.59	−22.90	2457802.38–2457825.37	3.557×10^{-3}
IC 4964	304.35	−73.89	39.26	−18.72	−21.34	2457802.38–2457825.37	2.934×10^{-3}
IC 4885	295.97	−60.65	29.92	−18.39	−21.35	2457802.38–2457825.37	2.844×10^{-3}
UGC 04845	138.11	9.96	30.18	−18.33	−20.68	2457802.38–2457825.37	2.502×10^{-3}
ESO 027-003	328.43	−81.65	30.64	−18.88	−18.75	2457802.38–2457825.37	2.216×10^{-3}
ESO 027–008	335.77	−80.00	21.88	−18.73	−22.39	2457802.38–2457825.37	2.100×10^{-3}
ESO 027-001	328.11	−81.53	29.92	−20.10	−23.21	2457802.38–2457825.37	1.780×10^{-3}

Note. The table columns provide the galaxy name, coordinates, distance, *B*- and *K*-band magnitudes, observing window, and the score from our ranking algorithm. The cumulative score is 0.704.

Table 5
Galaxies Observed after Trigger G275404 (with the Preliminary Bayestar Localization map)

Name (1)	R.A.(J2000) (2)	Decl.(J2000) (3)	Dist(Mpc) (4)	*B*(mag) (5)	*K*(mag) (6)	Obs_Window(JD) (7)	Score (8)
NGC 3923	177.76	−28.81	22.91	−20.97	−25.30	2457810.63–2457821.57	4.229×10^{-2}
NGC 3904	177.30	−29.28	28.31	−20.53	−24.58	2457810.63–2457821.57	3.748×10^{-2}
ESO 440-027	178.35	−28.55	18.53	−18.93	−21.74	2457810.63–2457821.57	3.080×10^{-2}
ESO 440-011	177.19	−28.29	21.88	−19.21	−18.05	2457810.63–2457821.57	2.991×10^{-2}
IC 3010	181.99	−30.34	25.87	−19.21	−22.86	2457810.63–2457821.57	2.848×10^{-2}
IC 3005	181.81	−30.02	24.32	−19.01	−21.96	2457810.63–2457821.57	2.618×10^{-2}
NGC 4105	181.67	−29.76	26.55	−20.32	−24.60	2457810.63–2457821.57	2.421×10^{-2}
ESO 441-014	182.56	−30.08	24.67	−18.60	−19.56	2457810.63–2457821.57	2.245×10^{-2}
IC 3253	185.94	−34.62	34.67	−21.00	−23.59	2457810.63–2457821.57	2.235×10^{-2}
IC 2996	181.45	−29.97	21.88	−18.47	−20.65	2457810.63–2457821.57	2.205×10^{-2}
NGC 3885	176.69	−27.92	21.88	−19.72	−23.33	2457810.63–2457821.57	2.126×10^{-2}
IC 0764	182.56	−29.74	21.18	−20.13	−21.92	2457810.63–2457821.57	2.064×10^{-2}
ESO 440-004	176.42	−28.37	22.93	−18.82	−18.47	2457810.63–2457821.57	1.781×10^{-2}
ESO 441-017	182.78	−31.13	24.24	−19.97	−21.10	2457810.63–2457821.57	1.721×10^{-2}
IC 3015	182.25	−31.52	24.21	−19.53	−23.11	2457810.63–2457821.57	1.707×10^{-2}
NGC 4304	185.55	−33.48	34.67	−20.24	−23.65	2457810.63–2457821.57	1.664×10^{-2}
NGC 3459	163.68	−17.04	31.61	−20.25	−22.44	2457810.63–2457821.57	1.566×10^{-2}
IC 0760	181.47	−29.29	25.37	−19.23	−22.63	2457810.63–2457821.57	1.539×10^{-2}
PGC 086291	283.00	11.88	38.02	−20.63	−24.07	2457810.63–2457821.57	1.298×10^{-2}
ESO 440-049	181.39	−31.42	24.24	−18.99	−20.12	2457810.63–2457821.57	1.209×10^{-2}
ESO 380-019	185.51	−35.79	38.02	−20.37	−24.24	2457810.63–2457821.57	1.140×10^{-2}
PGC 033108	164.91	−15.53	35.63	−20.04	−21.28	2457810.63–2457821.57	1.082×10^{-2}
NGC 3321	159.71	−11.65	33.88	−19.85	−22.17	2457810.63–2457821.57	1.002×10^{-2}
NGC 3936	178.09	−26.91	18.62	−19.55	−22.28	2457810.63–2457821.57	9.942×10^{-3}
ESO 380-050	189.59	−35.62	38.02	−20.13	−20.51	2457810.63–2457821.57	8.576×10^{-3}
ESO 504-028	178.73	−27.25	22.24	−18.89	−20.30	2457810.63–2457821.57	7.981×10^{-3}
NGC 4947	196.33	−35.34	27.80	−20.32	−23.20	2457810.63–2457821.57	7.905×10^{-3}
PGC 032091	161.30	−10.06	27.64	−18.64	−20.17	2457810.63–2457821.57	6.998×10^{-3}
ESO 440-038	180.43	−31.70	26.65	−19.10	−22.02	2457810.63–2457821.57	6.523×10^{-3}
NGC 3375	161.75	−9.94	28.87	−19.54	−22.53	2457810.63–2457821.57	5.771×10^{-3}
NGC 3361	161.12	−11.21	24.21	−19.13	−21.86	2457810.63–2457821.57	5.756×10^{-3}
PGC 031979	160.90	−9.86	24.21	−18.32	−19.86	2457810.63–2457821.57	5.567×10^{-3}
NGC 3055	148.83	4.27	25.35	−19.54	−22.53	2457810.63–2457821.57	5.334×10^{-3}
UGC 05347	149.32	4.53	29.92	−19.03	−20.24	2457810.63–2457821.57	5.171×10^{-3}
IC 2627	167.47	−23.73	24.21	−19.62	−22.93	2457810.63–2457821.57	5.125×10^{-3}
ESO 441-012	182.36	−32.52	24.21	−18.28	−21.73	2457810.63–2457821.57	4.921×10^{-3}
NGC 5121	201.19	−37.68	20.80	−19.59	−23.13	2457810.63–2457821.57	4.883×10^{-3}
NGC 3044	148.42	1.58	21.68	−19.85	−22.70	2457810.63–2457821.57	4.768×10^{-3}
NGC 3617	169.46	−26.13	25.61	−18.91	−22.26	2457810.63–2457821.57	4.067×10^{-3}
IC 0630	159.64	−7.17	25.85	−19.72	−23.41	2457810.63–2457821.57	3.970×10^{-3}
ESO 381-029	194.12	−36.37	29.54	−19.39	−22.62	2457810.63–2457821.57	3.914×10^{-3}
ESO 440-037	179.82	−28.90	22.99	−18.26	−20.92	2457810.63–2457821.57	3.717×10^{-3}
IC 2995	181.45	−27.94	16.75	−19.42	−21.80	2457810.63–2457821.57	3.706×10^{-3}
NGC 3673	171.30	−26.74	17.38	−19.20	−22.65	2457810.63–2457821.57	3.586×10^{-3}
ESO 324-044	204.53	−39.84	34.51	−19.70	−21.85	2457810.63–2457821.57	3.514×10^{-3}
NGC 3511	165.85	−23.09	12.25	−19.64	−22.37	2457810.63–2457821.57	3.494×10^{-3}
ESO 324-023	201.87	−38.18	14.26	−18.21	−19.15	2457810.63–2457821.57	3.151×10^{-3}
UGC 05376	150.11	3.37	29.92	−18.81	−22.60	2457810.63–2457821.57	2.772×10^{-3}
ESO 569-014	162.85	−19.89	24.77	−19.33	−20.98	2457810.63–2457821.57	2.756×10^{-3}
ESO 381-038	195.02	−34.43	28.37	−18.70	−20.39	2457810.63–2457821.57	2.425×10^{-3}

Note. The table columns provide the galaxy name, coordinates, distance, *B*- and *K*-band magnitudes, observing window, and the score from our ranking algorithm. The cumulative sore is 0.621.

Table 6
Galaxies Observed after Trigger G275404 (with the Updated LALInference Localization map)

Name (1)	R.A.(J2000) (2)	Decl.(J2000) (3)	Dist(Mpc) (4)	*B*(mag) (5)	*K*(mag) (6)	Obs_Window(JD) (7)	Score (8)
NGC 3923	177.76	−28.81	22.91	−20.97	−25.30	2457821.57–2457825.39	1.209×10^{-2}
NGC 3904	177.30	−29.28	28.31	−20.53	−24.58	2457821.57–2457825.39	1.112×10^{-2}
ESO 380-006	183.89	−35.63	38.93	−21.31	−24.79	2457821.57–2457825.39	8.775×10^{-3}
NGC 4603	190.23	−40.98	33.11	−21.20	−24.23	2457821.57–2457825.39	8.708×10^{-3}
NGC 4696	192.21	−41.31	35.48	−21.47	−25.61	2457821.57–2457825.39	7.815×10^{-3}
IC 3253	185.94	−34.62	34.67	−21.00	−23.59	2457821.57–2457825.39	7.541×10^{-3}
NGC 4105	181.67	−29.76	26.55	−20.32	−24.60	2457821.57–2457825.39	7.295×10^{-3}
IC 0764	182.56	−29.74	21.18	−20.13	−21.92	2457821.57–2457825.39	6.613×10^{-3}
NGC 4373A	186.41	−39.32	37.33	−20.63	−24.06	2457821.57–2457825.39	5.834×10^{-3}
NGC 3585	168.32	−26.75	20.05	−20.77	−24.81	2457821.57–2457825.39	5.682×10^{-3}
ESO 380-019	185.51	−35.79	38.02	−20.37	−24.24	2457821.57–2457825.39	5.256×10^{-3}
IC 3370	186.90	−39.34	26.79	−20.37	−24.28	2457821.57–2457825.39	5.116×10^{-3}
NGC 4304	185.55	−33.48	34.67	−20.24	−23.65	2457821.57–2457825.39	4.928×10^{-3}
ESO 321-025	185.43	−39.77	29.38	−20.32	−22.58	2457821.57–2457825.39	4.578×10^{-3}
NGC 3459	163.68	−17.04	31.61	−20.25	−22.44	2457821.57–2457825.39	4.299×10^{-3}
NGC 5365	209.46	−43.93	32.36	−20.35	−24.63	2457821.57–2457825.39	4.286×10^{-3}
PGC 086291	283.00	11.88	38.02	−20.63	−24.07	2457821.57–2457825.39	4.207×10^{-3}
NGC 5365A	209.16	−44.01	36.98	−20.27	−24.00	2457821.57–2457825.39	3.973×10^{-3}
NGC 5078	199.96	−27.41	27.67	−21.24	−25.09	2457821.57–2457825.39	3.946×10^{-3}
ESO 320-026	177.46	−38.78	38.02	−20.92	−24.22	2457821.57–2457825.39	3.820×10^{-3}
NGC 5101	200.44	−27.43	24.21	−20.68	−24.76	2457821.57–2457825.39	3.675×10^{-3}
IC 2977	178.81	−37.70	39.01	−20.82	−23.84	2457821.57–2457825.39	3.626×10^{-3}
ESO 320-030	178.30	−39.13	38.02	−20.25	−23.69	2457821.57–2457825.39	3.508×10^{-3}
NGC 5643	218.17	−44.17	18.45	−21.16	−24.16	2457821.57–2457825.39	3.359×10^{-3}
ESO 442-026	193.06	−29.84	34.94	−20.71	−24.29	2457821.57–2457825.39	3.129×10^{-3}
NGC 5266	205.76	−48.17	38.02	−21.14	−25.42	2457821.57–2457825.39	3.090×10^{-3}
ESO 221-012	207.89	−48.08	38.02	−20.10	−21.99	2457821.57–2457825.39	3.084×10^{-3}
ESO 221-014	208.03	−48.17	35.81	−20.29	−23.14	2457821.57–2457825.39	3.042×10^{-3}
NGC 3169	153.56	3.47	18.45	−20.30	−24.05	2457821.57–2457825.39	2.957×10^{-3}
NGC 3742	173.89	−37.96	38.61	−20.57	−24.29	2457821.57–2457825.39	2.919×10^{-3}
NGC 4767	193.47	−39.71	32.81	−20.38	−24.36	2457821.57–2457825.39	2.858×10^{-3}
NGC 3749	173.97	−38.00	38.02	−20.80	−24.20	2457821.57–2457825.39	2.840×10^{-3}
NGC 4947	196.33	−35.34	27.80	−20.32	−23.20	2457821.57–2457825.39	2.775×10^{-3}
ESO 380-050	189.59	−35.62	38.02	−20.13	−20.51	2457821.57–2457825.39	2.689×10^{-3}
NGC 5061	199.52	−26.84	24.21	−20.82	−24.63	2457821.57–2457825.39	2.530×10^{-3}
NGC 3783	174.76	−37.74	38.02	−20.50	−24.25	2457821.57–2457825.39	2.483×10^{-3}
PGC 046029	198.58	−46.12	36.98	−20.36	−24.31	2457821.57–2457825.39	2.469×10^{-3}
NGC 5266A	205.15	−48.34	38.02	−20.75	−22.20	2457821.57–2457825.39	2.425×10^{-3}
ESO 321-016	183.86	−38.14	38.02	−20.15	−21.98	2457821.57–2457825.39	2.386×10^{-3}
ESO 221-010	207.74	−49.06	38.02	−20.53	−23.65	2457821.57–2457825.39	2.363×10^{-3}
NGC 5063	199.61	−35.35	33.39	−20.35	−23.28	2457821.57–2457825.39	2.313×10^{-3}
IC 4444	217.91	−43.42	25.35	−20.22	−23.42	2457821.57–2457825.39	2.270×10^{-3}
NGC 3706	172.44	−36.39	38.02	−21.00	−25.00	2457821.57–2457825.39	2.221×10^{-3}
ESO 271-022	213.38	−45.41	38.14	−20.89	−23.12	2457821.57–2457825.39	2.180×10^{-3}
IC 4214	199.43	−32.10	28.84	−20.59	−24.09	2457821.57–2457825.39	2.170×10^{-3}
NGC 6574	272.96	14.98	38.91	−20.99	−24.54	2457821.57–2457825.39	2.094×10^{-3}
NGC 3115	151.31	−7.72	10.33	−20.13	−24.19	2457821.57–2457825.39	1.955×10^{-3}
ESO 221-020	209.60	−48.48	38.29	−20.15	−23.63	2457821.57–2457825.39	1.948×10^{-3}
ESO 269-057	197.52	−46.44	36.98	−20.63	−24.06	2457821.57–2457825.39	1.900×10^{-3}
NGC 5688	219.90	−45.02	30.90	−20.59	−24.13	2457821.57–2457825.39	1.860×10^{-3}
ESO 320-031	178.53	−39.87	38.18	−20.45	−24.87	2457821.57–2457825.39	1.825×10^{-3}
NGC 6570	272.78	14.09	33.42	−20.22	−22.75	2457821.57–2457825.39	1.714×10^{-3}
IC 4197	197.02	−23.80	34.10	−20.24	−23.39	2457821.57–2457825.39	1.657×10^{-3}
NGC 5188	202.87	−34.79	28.84	−20.20	−23.78	2457821.57–2457825.39	1.616×10^{-3}
ESO 221-025	211.90	−48.39	38.93	−20.26	−19.44	2457821.57–2457825.39	1.571×10^{-3}
NGC 5219	204.67	−45.86	36.98	−20.40	−22.88	2457821.57–2457825.39	1.469×10^{-3}
ESO 221-026	212.10	−47.97	20.31	−20.13	−24.00	2457821.57–2457825.39	1.389×10^{-3}
NGC 5483	212.60	−43.32	24.21	−20.22	−23.46	2457821.57–2457825.39	1.381×10^{-3}
NGC 3962	178.67	−13.97	35.32	−21.24	−25.07	2457821.57–2457825.39	1.362×10^{-3}
ESO 507-032	193.06	−26.30	20.82	−20.22	−22.30	2457821.57–2457825.39	1.346×10^{-3}
NGC 3672	171.26	−9.80	23.66	−20.77	−23.60	2457821.57–2457825.39	1.306×10^{-3}
NGC 6555	271.96	17.60	33.42	−20.82	−22.79	2457821.57–2457825.39	1.303×10^{-3}
NGC 4993	197.45	−23.38	39.99	−20.20	−23.42	2457821.57–2457825.39	1.279×10^{-3}

Table 6
(Continued)

Name (1)	R.A.(J2000) (2)	Decl.(J2000) (3)	Dist(Mpc) (4)	*B*(mag) (5)	*K*(mag) (6)	Obs_Window(JD) (7)	Score (8)
NGC 4444	187.15	−43.26	36.98	−20.63	−23.43	2457821.57–2457825.39	1.269×10^{-3}
ESO 386-039	224.11	−37.60	36.98	−20.10	−22.89	2457821.57–2457825.39	1.241×10^{-3}
ESO 176-006	224.29	−54.39	38.01	−21.52	−24.43	2457821.57–2457825.39	1.213×10^{-3}
NGC 2967	145.51	0.34	29.92	−20.24	−23.50	2457821.57–2457825.39	1.209×10^{-3}
NGC 5156	202.18	−48.92	36.98	−20.94	−24.11	2457821.57–2457825.39	1.113×10^{-3}
ESO 377-024	168.14	−36.43	38.21	−20.23	−22.95	2457821.57–2457825.39	1.081×10^{-3}
NGC 6384	263.10	7.06	25.94	−21.26	−24.54	2457821.57–2457825.39	1.062×10^{-3}
NGC 3368	161.69	11.82	10.47	−20.18	−23.78	2457821.57–2457825.39	1.021×10^{-3}
NGC 4462	187.34	−23.17	23.12	−20.12	−23.36	2457821.57–2457825.39	9.324×10^{-4}
NGC 3338	160.53	13.75	24.43	−20.95	−23.81	2457821.57–2457825.39	9.297×10^{-4}
NGC 4976	197.16	−49.51	17.30	−20.90	−24.34	2457821.57–2457825.39	9.070×10^{-4}
IC 4351	209.48	−29.32	27.54	−20.80	−24.18	2457821.57–2457825.39	8.962×10^{-4}
ESO 385-030	217.33	−33.45	34.33	−20.42	−24.09	2457821.57–2457825.39	8.081×10^{-4}
2MASXJ133706182953185	204.25	−29.87	4.92	−20.26	−23.84	2457821.57–2457825.39	7.861×10^{-4}
NGC 4219	184.11	−43.32	20.99	−20.51	−23.52	2457821.57–2457825.39	7.476×10^{-4}
NGC 4835	194.53	−46.26	20.14	−20.22	−23.34	2457821.57–2457825.39	7.294×10^{-4}
NGC 5494	213.10	−30.64	31.19	−20.19	−23.50	2457821.57–2457825.39	6.711×10^{-4}
PGC 054411	228.64	−52.99	19.36	−20.60	−24.25	2457821.57–2457825.39	5.852×10^{-4}
ESO 175-005	214.45	−52.83	37.36	−20.38	−20.29	2457821.57–2457825.39	5.068×10^{-4}
NGC 5085	200.07	−24.44	24.21	−20.32	−23.00	2457821.57–2457825.39	4.894×10^{-4}
NGC 4112	181.79	−40.21	34.67	−20.54	−23.50	2457821.57–2457825.39	4.340×10^{-4}
NGC 2992	146.43	−14.33	28.84	−20.39	−23.70	2457821.57–2457825.39	2.813×10^{-4}

Note. The table columns provide the galaxy name, coordinates, distance, *B*- and *K*-band magnitudes, observing window, and the score from our ranking algorithm. The cumulative sore is 0.243.

Table 7
Galaxies Observed after Trigger G275697 (with the Preliminary Bayestar Localization map)

Name (1)	R.A.(J2000) (2)	Decl.(J2000) (3)	Dist(Mpc) (4)	*B*(mag) (5)	*K*(mag) (6)	Obs_Window(JD) (7)	Score (8)
NGC 3742	173.89	−37.96	38.61	−20.57	−24.29	2457812.34–2457820.41	4.087×10^{-2}
NGC 3749	173.97	−38.00	38.02	−20.80	−24.20	2457812.34–2457820.41	3.951×10^{-2}
ESO 320-026	177.46	−38.78	38.02	−20.92	−24.22	2457812.34–2457820.41	3.305×10^{-2}
ESO 320-004	173.68	−38.25	38.02	−19.46	−21.31	2457812.34–2457820.41	3.203×10^{-2}
ESO 320-027	177.60	−38.65	37.64	−19.93	−20.41	2457812.34–2457820.41	3.092×10^{-2}
ESO 320-024	177.36	−38.83	38.89	−19.55	−21.80	2457812.34–2457820.41	3.087×10^{-2}
NGC 3783	174.76	−37.74	38.02	−20.50	−24.25	2457812.34–2457820.41	2.898×10^{-2}
ESO 320-030	178.30	−39.13	38.02	−20.25	−23.69	2457812.34–2457820.41	2.888×10^{-2}
NGC 3706	172.44	−36.39	38.02	−21.00	−25.00	2457812.34–2457820.41	2.707×10^{-2}
ESO 320-031	178.53	−39.87	38.18	−20.45	−24.87	2457812.34–2457820.41	1.918×10^{-2}
NGC 3606	169.06	−33.83	37.68	−20.01	−23.49	2457812.34–2457820.41	1.455×10^{-2}
ESO 378-012	174.26	−36.82	37.94	−19.51	−22.62	2457812.34–2457820.41	1.423×10^{-2}
ESO 221-004	207.47	−48.58	37.96	−19.41	−19.63	2457812.34–2457820.41	1.383×10^{-2}
ESO 377-029	168.66	−33.91	38.56	−19.75	−23.41	2457812.34–2457820.41	1.320×10^{-2}
ESO 378-020	176.82	−37.55	39.46	−19.90	−23.44	2457812.34–2457820.41	1.240×10^{-2}
ESO 221-003	207.44	−48.75	38.02	−19.49	−21.96	2457812.34–2457820.41	1.211×10^{-2}
NGC 5266	205.76	−48.17	38.02	−21.14	−25.42	2457812.34–2457820.41	1.210×10^{-2}
NGC 3903	177.26	−37.52	38.02	−19.89	−22.63	2457812.34–2457820.41	1.205×10^{-2}
PGC 049119	207.62	−48.28	38.02	−20.06	−22.40	2457812.34–2457820.41	1.121×10^{-2}
ESO 377-024	168.14	−36.43	38.21	−20.23	−22.95	2457812.34–2457820.41	1.119×10^{-2}
NGC 5266A	205.15	−48.34	38.02	−20.75	−22.20	2457812.34–2457820.41	1.119×10^{-2}
ESO 221-010	207.74	−49.06	38.02	−20.53	−23.65	2457812.34–2457820.41	1.118×10^{-2}
NGC 4976	197.16	−49.51	17.30	−20.90	−24.34	2457812.34–2457820.41	1.118×10^{-2}
NGC 3573	167.83	−36.88	37.18	−19.87	−24.02	2457812.34–2457820.41	1.070×10^{-2}
ESO 220-026	204.94	−48.30	38.75	−19.41	−19.80	2457812.34–2457820.41	1.040×10^{-2}
NGC 5156	202.18	−48.92	36.98	−20.94	−24.11	2457812.34–2457820.41	1.037×10^{-2}
IC 2977	178.81	−37.70	39.01	−20.82	−23.84	2457812.34–2457820.41	1.005×10^{-2}
NGC 4219	184.11	−43.32	20.99	−20.51	−23.52	2457812.34–2457820.41	9.649×10^{-3}
ESO 219-022	195.60	−49.47	23.56	−19.68	−21.99	2457812.34–2457820.41	9.184×10^{-3}
ESO 221-014	208.03	−48.17	35.81	−20.29	−23.14	2457812.34–2457820.41	9.143×10^{-3}
ESO 377-021	167.74	−35.98	32.81	−19.45	−22.20	2457812.34–2457820.41	9.138×10^{-3}

Table 7
(Continued)

Name (1)	R.A.(J2000) (2)	Decl.(J2000) (3)	Dist(Mpc) (4)	*B*(mag) (5)	*K*(mag) (6)	Obs_Window(JD) (7)	Score (8)
ESO 221-012	207.89	−48.08	38.02	−20.10	−21.99	2457812.34–2457820.41	8.879×10^{-3}
IC 3896A	193.88	−50.07	27.67	−20.00	−20.30	2457812.34–2457820.41	8.153×10^{-3}
NGC 4444	187.15	−43.26	36.98	−20.63	−23.43	2457812.34–2457820.41	8.134×10^{-3}
ESO 269-057	197.52	−46.44	36.98	−20.63	−24.06	2457812.34–2457820.41	7.846×10^{-3}
IC 3896	194.18	−50.35	27.67	−20.51	−24.42	2457812.34–2457820.41	7.778×10^{-3}
ESO 220-009	201.72	−48.16	37.46	−19.43	−22.70	2457812.34–2457820.41	7.578×10^{-3}
PGC 046029	198.58	−46.12	36.98	−20.36	−24.31	2457812.34–2457820.41	6.891×10^{-3}
ESO 269-090	200.21	−47.22	37.03	−19.96	−23.35	2457812.34–2457820.41	6.747×10^{-3}
ESO 269-085	200.00	−47.28	28.31	−19.46	−23.30	2457812.34–2457820.41	6.448×10^{-3}
ESO 221-020	209.60	−48.48	38.29	−20.15	−23.63	2457812.34–2457820.41	5.942×10^{-3}
ESO 377-019	167.69	−35.35	37.40	−19.43	−21.72	2457812.34–2457820.41	5.848×10^{-3}
NGC 4835	194.53	−46.26	20.14	−20.22	−23.34	2457812.34–2457820.41	4.894×10^{-3}
ESO 220-023	204.33	−49.75	38.02	−19.76	−23.23	2457812.34–2457820.41	3.982×10^{-3}
NGC 3115	151.31	−7.72	10.33	−20.13	−24.19	2457812.34–2457820.41	3.759×10^{-3}
ESO 321-021	185.07	−40.39	39.65	−20.07	−22.64	2457812.34–2457820.41	3.570×10^{-3}
NGC 4573	189.43	−43.62	37.42	−19.63	−23.22	2457812.34–2457820.41	3.532×10^{-3}
ESO 175-005	214.45	−52.83	37.36	−20.38	−20.29	2457812.34–2457820.41	3.510×10^{-3}
ESO 268-027	189.63	−42.86	38.42	−19.37	−22.45	2457812.34–2457820.41	3.454×10^{-3}
ESO 319-016	170.53	−38.07	38.22	−19.68	−20.96	2457812.34–2457820.41	3.159×10^{-3}
NGC 2967	145.51	0.34	29.92	−20.24	−23.50	2457812.34–2457820.41	2.765×10^{-3}
ESO 267-016	181.59	−44.45	39.26	−19.36	−22.30	2457812.34–2457820.41	2.637×10^{-3}
ESO 221-032	213.04	−49.39	36.98	−19.87	−23.86	2457812.34–2457820.41	2.309×10^{-3}
ESO 321-005	181.45	−38.85	36.46	−19.75	−22.20	2457812.34–2457820.41	2.237×10^{-3}
NGC 2974	145.64	−3.70	21.48	−20.01	−25.41	2457812.34–2457820.41	2.202×10^{-3}
ESO 438-005	167.24	−28.37	26.18	−19.38	−19.64	2457812.34–2457820.41	2.110×10^{-3}
ESO 268-044	192.18	−45.01	37.67	−19.35	−22.26	2457812.34–2457820.41	2.056×10^{-3}
PGC 166337	216.65	−52.73	38.39	−19.57	−22.29	2457812.34–2457820.41	2.045×10^{-3}
NGC 4112	181.79	−40.21	34.67	−20.54	−23.50	2457812.34–2457820.41	1.912×10^{-3}

Note. The table columns provide the galaxy name, coordinates, distance, *B*- and *K*-band magnitudes, observing window, and the score from our ranking algorithm. The cumulative score is 0.681.

Table 8
Galaxies Observed after Trigger G275697 (with the Updated LALInference Localization map)

Name (1)	R.A.(J2000) (2)	Decl.(J2000) (3)	Dist(Mpc) (4)	*B*(mag) (5)	*K*(mag) (6)	Obs_Window(JD) (7)	Score (8)
NGC 3742	173.89	−37.96	38.61	−20.57	−24.29	2457820.41–2457825.39	1.823×10^{-2}
NGC 3749	173.97	−38.00	38.02	−20.80	−24.20	2457820.41–2457825.39	1.761×10^{-2}
NGC 3557B	167.38	−37.35	36.98	−20.06	−23.75	2457820.41–2457825.39	1.554×10^{-2}
NGC 3573	167.83	−36.88	37.18	−19.87	−24.02	2457820.41–2457825.39	1.538×10^{-2}
ESO 320-004	173.68	−38.25	38.02	−19.46	−21.31	2457820.41–2457825.39	1.495×10^{-2}
ESO 320-026	177.46	−38.78	38.02	−20.92	−24.22	2457820.41–2457825.39	1.454×10^{-2}
NGC 3564	167.65	−37.55	36.98	−20.08	−23.89	2457820.41–2457825.39	1.409×10^{-2}
ESO 320-027	177.60	−38.65	37.64	−19.93	−20.41	2457820.41–2457825.39	1.399×10^{-2}
ESO 320-024	177.36	−38.83	38.89	−19.55	−21.80	2457820.41–2457825.39	1.348×10^{-2}
NGC 3533	166.78	−37.17	36.88	−20.39	−23.59	2457820.41–2457825.39	1.345×10^{-2}
ESO 320-030	178.30	−39.13	38.02	−20.25	−23.69	2457820.41–2457825.39	1.293×10^{-2}
ESO 377-024	168.14	−36.43	38.21	−20.23	−22.95	2457820.41–2457825.39	1.241×10^{-2}
NGC 3783	174.76	−37.74	38.02	−20.50	−24.25	2457820.41–2457825.39	1.211×10^{-2}
NGC 3706	172.44	−36.39	38.02	−21.00	−25.00	2457820.41–2457825.39	1.152×10^{-2}
ESO 377-010	166.63	−37.65	36.98	−20.37	−23.82	2457820.41–2457825.39	1.142×10^{-2}
ESO 377-021	167.74	−35.98	32.81	−19.45	−22.20	2457820.41–2457825.39	9.741×10^{-3}
ESO 320-031	178.53	−39.87	38.18	−20.45	−24.87	2457820.41–2457825.39	8.197×10^{-3}
ESO 221-004	207.47	−48.58	37.96	−19.41	−19.63	2457820.41–2457825.39	8.051×10^{-3}
PGC 049119	207.62	−48.28	38.02	−20.06	−22.40	2457820.41–2457825.39	7.170×10^{-3}
NGC 5266	205.76	−48.17	38.02	−21.14	−25.42	2457820.41–2457825.39	7.125×10^{-3}
IC 2977	178.81	−37.70	39.01	−20.82	−23.84	2457820.41–2457825.39	7.118×10^{-3}
ESO 437-033	159.99	−30.19	36.98	−19.39	−22.91	2457820.41–2457825.39	6.960×10^{-3}
ESO 221-003	207.44	−48.75	38.02	−19.49	−21.96	2457820.41–2457825.39	6.813×10^{-3}
NGC 3903	177.26	−37.52	38.02	−19.89	−22.63	2457820.41–2457825.39	6.536×10^{-3}

Table 8
(Continued)

Name (1)	R.A.(J2000) (2)	Decl.(J2000) (3)	Dist(Mpc) (4)	*B*(mag) (5)	*K*(mag) (6)	Obs_Window(JD) (7)	Score (8)
NGC 3606	169.06	−33.83	37.68	−20.01	−23.49	2457820.41–2457825.39	6.447×10^{-3}
ESO 437-030	159.81	−30.30	39.81	−20.54	−23.69	2457820.41–2457825.39	6.402×10^{-3}
NGC 5266A	205.15	−48.34	38.02	−20.75	−22.20	2457820.41–2457825.39	6.342×10^{-3}
NGC 4976	197.16	−49.51	17.30	−20.90	−24.34	2457820.41–2457825.39	6.313×10^{-3}
ESO 377-029	168.66	−33.91	38.56	−19.75	−23.41	2457820.41–2457825.39	6.272×10^{-3}
ESO 221-014	208.03	−48.17	35.81	−20.29	−23.14	2457820.41–2457825.39	6.121×10^{-3}
ESO 221-012	207.89	−48.08	38.02	−20.10	−21.99	2457820.41–2457825.39	6.086×10^{-3}
IC 3896	194.18	−50.35	27.67	−20.51	−24.42	2457820.41–2457825.39	6.075×10^{-3}
ESO 221-010	207.74	−49.06	38.02	−20.53	−23.65	2457820.41–2457825.39	6.065×10^{-3}
IC 3896A	193.88	−50.07	27.67	−20.00	−20.30	2457820.41–2457825.39	6.064×10^{-3}
ESO 378-020	176.82	−37.55	39.46	−19.90	−23.44	2457820.41–2457825.39	6.060×10^{-3}
NGC 5333	208.60	−48.51	35.81	−19.29	−24.40	2457820.41–2457825.39	5.944×10^{-3}
ESO 220-026	204.94	−48.30	38.75	−19.41	−19.80	2457820.41–2457825.39	5.909×10^{-3}
ESO 378-012	174.26	−36.82	37.94	−19.51	−22.62	2457820.41–2457825.39	5.898×10^{-3}
NGC 4603	190.23	−40.98	33.11	−21.20	−24.23	2457820.41–2457825.39	5.590×10^{-3}
ESO 176-006	224.29	−54.39	38.01	−21.52	−24.43	2457820.41–2457825.39	5.447×10^{-3}
ESO 219-022	195.60	−49.47	23.56	−19.68	−21.99	2457820.41–2457825.39	5.430×10^{-3}
ESO 377-019	167.69	−35.35	37.40	−19.43	−21.72	2457820.41–2457825.39	5.276×10^{-3}
NGC 4645	191.04	−41.75	29.92	−20.08	−23.94	2457820.41–2457825.39	5.259×10^{-3}
NGC 5156	202.18	−48.92	36.98	−20.94	−24.11	2457820.41–2457825.39	5.217×10^{-3}
NGC 4603C	190.18	−40.76	38.83	−19.60	−23.11	2457820.41–2457825.39	5.217×10^{-3}
NGC 4603A	189.90	−40.74	30.34	−19.45	−22.33	2457820.41–2457825.39	4.926×10^{-3}
ESO 269-060	197.75	−46.22	36.98	−19.28	−22.71	2457820.41–2457825.39	4.822×10^{-3}
ESO 269-057	197.52	−46.44	36.98	−20.63	−24.06	2457820.41–2457825.39	4.668×10^{-3}
PGC 046029	198.58	−46.12	36.98	−20.36	−24.31	2457820.41–2457825.39	4.650×10^{-3}
ESO 321-025	185.43	−39.77	29.38	−20.32	−22.58	2457820.41–2457825.39	4.503×10^{-3}
NGC 4444	187.15	−43.26	36.98	−20.63	−23.43	2457820.41–2457825.39	4.350×10^{-3}
NGC 4219	184.11	−43.32	20.99	−20.51	−23.52	2457820.41–2457825.39	4.316×10^{-3}
NGC 4696	192.21	−41.31	35.48	−21.47	−25.61	2457820.41–2457825.39	4.266×10^{-3}
ESO 322-045	190.01	−42.04	38.93	−19.98	−23.00	2457820.41–2457825.39	4.182×10^{-3}
ESO 221-020	209.60	−48.48	38.29	−20.15	−23.63	2457820.41–2457825.39	4.012×10^{-3}
NGC 4373A	186.41	−39.32	37.33	−20.63	−24.06	2457820.41–2457825.39	3.995×10^{-3}
NGC 4575	189.46	−40.54	29.11	−19.83	−22.97	2457820.41–2457825.39	3.941×10^{-3}
ESO 220-009	201.72	−48.16	37.46	−19.43	−22.70	2457820.41–2457825.39	3.927×10^{-3}
PGC 027810	145.82	−9.95	38.39	−20.05	−22.28	2457820.41–2457825.39	3.883×10^{-3}
ESO 269-090	200.21	−47.22	37.03	−19.96	−23.35	2457820.41–2457825.39	3.813×10^{-3}
NGC 3585	168.32	−26.75	20.05	−20.77	−24.81	2457820.41–2457825.39	3.801×10^{-3}
ESO 269-085	200.00	−47.28	28.31	−19.46	−23.30	2457820.41–2457825.39	3.639×10^{-3}
ESO 321-021	185.07	−40.39	39.65	−20.07	−22.64	2457820.41–2457825.39	3.638×10^{-3}
ESO 269-078	199.16	−45.89	37.86	−19.27	−20.24	2457820.41–2457825.39	3.477×10^{-3}
ESO 221-022	210.05	−48.27	34.20	−19.30	−22.60	2457820.41–2457825.39	3.425×10^{-3}
ESO 322-042	189.67	−42.21	34.83	−19.61	−21.43	2457820.41–2457825.39	3.384×10^{-3}
NGC 2979	145.79	−10.38	38.02	−19.52	−23.39	2457820.41–2457825.39	3.232×10^{-3}
IC 3370	186.90	−39.34	26.79	−20.37	−24.28	2457820.41–2457825.39	3.112×10^{-3}
ESO 221-025	211.90	−48.39	38.93	−20.26	−19.44	2457820.41–2457825.39	2.954×10^{-3}
PGC 028308	147.56	−12.06	38.02	−20.07	−22.58	2457820.41–2457825.39	2.924×10^{-3}
ESO 322-027	188.68	−40.30	39.54	−20.03	−23.26	2457820.41–2457825.39	2.886×10^{-3}
ESO 319-016	170.53	−38.07	38.22	−19.68	−20.96	2457820.41–2457825.39	2.866×10^{-3}
ESO 268-027	189.63	−42.86	38.42	−19.37	−22.45	2457820.41–2457825.39	2.850×10^{-3}
ESO 437-014	159.22	−32.35	37.33	−20.16	−23.62	2457820.41–2457825.39	2.668×10^{-3}
NGC 4835	194.53	−46.26	20.14	−20.22	−23.34	2457820.41–2457825.39	2.576×10^{-3}
ESO 175-005	214.45	−52.83	37.36	−20.38	−20.29	2457820.41–2457825.39	2.427×10^{-3}
ESO 221-026	212.10	−47.97	20.31	−20.13	−24.00	2457820.41–2457825.39	2.364×10^{-3}
NGC 3208	154.92	−25.81	36.98	−19.63	−23.43	2457820.41–2457825.39	2.336×10^{-3}
NGC 3203	154.89	−26.70	32.36	−19.99	−23.69	2457820.41–2457825.39	2.250×10^{-3}
NGC 4573	189.43	−43.62	37.42	−19.63	−23.22	2457820.41–2457825.39	2.239×10^{-3}
ESO 376-009	160.51	−33.25	38.78	−19.67	−23.40	2457820.41–2457825.39	2.084×10^{-3}
ESO 321-010	182.93	−38.55	38.02	−19.66	−22.79	2457820.41–2457825.39	2.075×10^{-3}
ESO 321-019	184.27	−39.05	37.64	−19.77	−22.82	2457820.41–2457825.39	2.071×10^{-3}
PGC 054411	228.64	−52.99	19.36	−20.60	−24.25	2457820.41–2457825.39	2.049×10^{-3}
ESO 220-023	204.33	−49.75	38.02	−19.76	−23.23	2457820.41–2457825.39	2.033×10^{-3}
NGC 2974	145.64	−3.70	21.48	−20.01	−25.41	2457820.41–2457825.39	1.974×10^{-3}
ESO 270-006	200.49	−45.94	36.98	−19.95	−22.57	2457820.41–2457825.39	1.957×10^{-3}

Table 8
(Continued)

Name (1)	R.A.(J2000) (2)	Decl.(J2000) (3)	Dist(Mpc) (4)	*B*(mag) (5)	*K*(mag) (6)	Obs_Window(JD) (7)	Score (8)
ESO 321-005	181.45	−38.85	36.46	−19.75	−22.20	2457820.41–2457825.39	1.935×10^{-3}
NGC 3115	151.31	−7.72	10.33	−20.13	−24.19	2457820.41–2457825.39	1.896×10^{-3}
NGC 3717	172.88	−30.31	16.90	−19.94	−23.62	2457820.41–2457825.39	1.842×10^{-3}
ESO 321-016	183.86	−38.14	38.02	−20.15	−21.98	2457820.41–2457825.39	1.728×10^{-3}
ESO 322-020	187.30	−40.69	39.58	−19.39	−20.47	2457820.41–2457825.39	1.660×10^{-3}
NGC 2967	145.51	0.34	29.92	−20.24	−23.50	2457820.41–2457825.39	1.637×10^{-3}
ESO 267-016	181.59	−44.45	39.26	−19.36	−22.30	2457820.41–2457825.39	1.623×10^{-3}
NGC 5219	204.67	−45.86	36.98	−20.40	−22.88	2457820.41–2457825.39	1.547×10^{-3}
ESO 321-018	183.98	−38.09	38.65	−19.78	−19.60	2457820.41–2457825.39	1.450×10^{-3}
PGC 166337	216.65	−52.73	38.39	−19.57	−22.29	2457820.41–2457825.39	1.400×10^{-3}
ESO 221-032	213.04	−49.39	36.98	−19.87	−23.86	2457820.41–2457825.39	1.395×10^{-3}
ESO 438-005	167.24	−28.37	26.18	−19.38	−19.64	2457820.41–2457825.39	1.264×10^{-3}
PGC 166343	219.26	−54.04	38.04	−19.70	−21.29	2457820.41–2457825.39	1.197×10^{-3}
ESO 268-044	192.18	−45.01	37.67	−19.35	−22.26	2457820.41–2457825.39	1.175×10^{-3}
NGC 4112	181.79	−40.21	34.67	−20.54	−23.50	2457820.41–2457825.39	1.126×10^{-3}
NGC 4751	193.21	−42.66	26.19	−19.67	−23.86	2457820.41–2457825.39	1.102×10^{-3}
ESO 175-009	218.00	−55.47	39.26	−19.60	−24.01	2457820.41–2457825.39	1.070×10^{-3}
NGC 2775	137.58	7.04	17.30	−20.17	−24.15	2457820.41–2457825.39	1.053×10^{-3}
IC 2580	157.08	−31.52	36.98	−19.70	−22.80	2457820.41–2457825.39	1.036×10^{-3}
NGC 3511	165.85	−23.09	12.25	−19.64	−22.37	2457820.41–2457825.39	1.006×10^{-3}
NGC 2993	146.45	−14.37	28.84	−19.48	−22.17	2457820.41–2457825.39	9.519×10^{-4}
NGC 2992	146.43	−14.33	28.84	−20.39	−23.70	2457820.41–2457825.39	9.074×10^{-4}
IC 2627	167.47	−23.73	24.21	−19.62	−22.93	2457820.41–2457825.39	8.357×10^{-4}
ESO 569-014	162.85	−19.89	24.77	−19.33	−20.98	2457820.41–2457825.39	7.522×10^{-4}
NGC 3175	153.68	−28.87	13.87	−19.39	−22.92	2457820.41–2457825.39	7.353×10^{-4}
ESO 222-015	221.12	−49.40	29.92	−19.41	−18.95	2457820.41–2457825.39	6.982×10^{-4}
NGC 2947	144.02	−12.44	39.88	−19.37	−23.05	2457820.41–2457825.39	6.017×10^{-4}

Note. The table columns provide the galaxy name, coordinates, distance, *B*- and *K*-band magnitudes, observing window, and the score from our ranking algorithm. The cumulative sore is 0.574.

Table 9
Galaxies Observed after Trigger G277583

Name (1)	R.A.(J2000) (2)	Decl.(J2000) (3)	Dist(Mpc) (4)	*B*(mag) (5)	*K*(mag) (6)	Obs_Window(JD) (7)	Score (8)
NGC 1407	55.05	−18.58	28.84	−21.65	−25.60	2457826.53–2457847.24	1.595×10^{-2}
NGC 1400	54.88	−18.69	26.42	−20.17	−24.30	2457826.53–2457847.24	1.502×10^{-2}
NGC 1393	54.66	−18.43	23.89	−19.49	−22.71	2457826.53–2457847.24	1.293×10^{-2}
NGC 1421	55.62	−13.49	25.35	−21.11	−23.62	2457826.53–2457847.24	1.102×10^{-2}
NGC 1625	69.28	−3.30	36.98	−20.44	−20.41	2457826.53–2457847.24	8.936×10^{-3}
PGC 013646	55.73	−12.92	25.35	−19.62	−22.63	2457826.53–2457847.24	8.625×10^{-3}
IC 2098	72.68	−5.42	32.36	−19.77	−22.35	2457826.53–2457847.24	8.333×10^{-3}
NGC 1665	72.07	−5.43	33.10	−19.32	−23.34	2457826.53–2457847.24	6.994×10^{-3}
NGC 1681	72.96	−5.80	32.36	−19.20	−22.15	2457826.53–2457847.24	6.709×10^{-3}
NGC 1398	54.72	−26.34	24.77	−21.50	−25.47	2457826.53–2457847.24	6.696×10^{-3}
NGC 1387	54.24	−35.51	20.32	−19.54	−24.11	2457826.53–2457847.24	6.453×10^{-3}
NGC 1399	54.62	−35.45	19.95	−20.65	−25.19	2457826.53–2457847.24	6.184×10^{-3}
NGC 1389	54.30	−35.75	21.68	−19.29	−23.05	2457826.53–2457847.24	6.155×10^{-3}
NGC 1379	54.02	−35.44	20.05	−19.44	−23.27	2457826.53–2457847.24	6.142×10^{-3}
NGC 2339	107.09	18.78	37.84	−21.21	−24.38	2457826.53–2457847.24	6.076×10^{-3}
NGC 1404	54.72	−35.59	20.99	−20.41	−24.79	2457826.53–2457847.24	5.940×10^{-3}
NGC 1395	54.62	−23.03	24.10	−20.75	−25.02	2457826.53–2457847.24	5.370×10^{-3}
NGC 1380	54.11	−34.98	17.62	−20.13	−24.36	2457826.53–2457847.24	4.995×10^{-3}
NGC 6118	245.45	−2.28	20.99	−20.21	−22.91	2457826.53–2457847.24	4.859×10^{-3}
NGC 1784	76.36	−11.87	30.48	−20.50	−23.91	2457826.53–2457847.24	4.672×10^{-3}
NGC 1426	55.70	−22.11	24.10	−19.63	−23.24	2457826.53–2457847.24	4.664×10^{-3}
NGC 1666	72.14	−6.57	33.08	−19.63	−23.16	2457826.53–2457847.24	4.655×10^{-3}
PGC 016894	77.92	−14.79	27.42	−20.19	−22.00	2457826.53–2457847.24	4.305×10^{-3}
NGC 1332	51.57	−21.34	22.91	−20.63	−24.75	2457826.53–2457847.24	4.238×10^{-3}
NGC 1365	53.40	−36.14	17.95	−21.39	−24.90	2457826.53–2457847.24	4.218×10^{-3}

Table 9
(Continued)

Name (1)	R.A.(J2000) (2)	Decl.(J2000) (3)	Dist(Mpc) (4)	*B*(mag) (5)	*K*(mag) (6)	Obs_Window(JD) (7)	Score (8)
PGC 013716	56.00	−14.36	16.54	−19.22	−21.18	2457826.53–2457847.24	4.203×10^{-3}
NGC 1439	56.21	−21.92	26.67	−19.61	−23.56	2457826.53–2457847.24	3.870×10^{-3}
UGC 10288	243.60	−0.21	32.96	−19.99	−23.20	2457826.53–2457847.24	3.857×10^{-3}
NGC 1359	53.45	−19.49	38.91	−20.57	−21.78	2457826.53–2457847.24	3.801×10^{-3}
NGC 1325	51.11	−21.54	19.95	−19.72	−22.87	2457826.53–2457847.24	3.574×10^{-3}
NGC 1832	78.01	−15.69	25.12	−20.32	−23.61	2457826.53–2457847.24	3.294×10^{-3}
NGC 1427	55.58	−35.39	23.55	−19.92	−23.72	2457826.53–2457847.24	3.250×10^{-3}
PGC 016917	78.10	−14.36	29.78	−19.36	−20.51	2457826.53–2457847.24	3.248×10^{-3}
UGC 03258	77.68	0.41	35.13	−19.59	−22.37	2457826.53–2457847.24	3.063×10^{-3}
NGC 1888	80.64	−11.50	28.84	−20.40	−23.99	2457826.53–2457847.24	2.896×10^{-3}
NGC 6063	241.80	7.98	37.50	−19.48	−22.32	2457826.53–2457847.24	2.882×10^{-3}
NGC 4373A	186.41	−39.32	37.33	−20.63	−24.06	2457826.53–2457847.24	2.795×10^{-3}
ESO 380-006	183.89	−35.63	38.93	−21.31	−24.79	2457826.53–2457847.24	2.739×10^{-3}
NGC 1954	83.20	−14.06	38.02	−20.93	−23.80	2457826.53–2457847.24	2.636×10^{-3}
UGC 03587	103.48	19.30	23.99	−19.70	−21.31	2457826.53–2457847.24	2.569×10^{-3}
NGC 5962	234.13	16.61	30.20	−20.55	−23.87	2457826.53–2457847.24	2.492×10^{-3}
ESO 321-025	185.43	−39.77	29.38	−20.32	−22.58	2457826.53–2457847.24	2.469×10^{-3}
IC 3370	186.90	−39.34	26.79	−20.37	−24.28	2457826.53–2457847.24	2.402×10^{-3}
NGC 6106	244.70	7.41	24.66	−19.60	−22.34	2457826.53–2457847.24	2.400×10^{-3}
NGC 6014	238.99	5.93	31.19	−19.42	−22.67	2457826.53–2457847.24	2.386×10^{-3}
NGC 1297	49.81	−19.10	28.58	−19.68	−23.35	2457826.53–2457847.24	2.344×10^{-3}
NGC 1300	49.92	−19.41	14.52	−19.86	−23.25	2457826.53–2457847.24	2.291×10^{-3}
NGC 1353	53.01	−20.82	17.30	−19.36	−23.08	2457826.53–2457847.24	2.272×10^{-3}
IC 2977	178.81	−37.70	39.01	−20.82	−23.84	2457826.53–2457847.24	2.268×10^{-3}
NGC 1532	63.02	−32.87	17.30	−20.54	−24.46	2457826.53–2457847.24	2.197×10^{-3}
NGC 5970	234.62	12.19	26.06	−20.13	−23.26	2457826.53–2457847.24	2.195×10^{-3}
ESO 322-027	188.68	−40.30	39.54	−20.03	−23.26	2457826.53–2457847.24	2.058×10^{-3}
NGC 1436	55.90	−35.85	19.86	−19.30	−22.46	2457826.53–2457847.24	2.048×10^{-3}
NGC 1357	53.32	−13.66	25.35	−19.68	−23.60	2457826.53–2457847.24	2.030×10^{-3}
IC 0407	79.43	−15.52	35.81	−20.24	−22.86	2457826.53–2457847.24	2.021×10^{-3}
ESO 321-016	183.86	−38.14	38.02	−20.15	−21.98	2457826.53–2457847.24	2.004×10^{-3}
NGC 1537	63.42	−31.65	23.23	−20.21	−24.10	2457826.53–2457847.24	1.965×10^{-3}
ESO 321-018	183.98	−38.09	38.65	−19.78	−19.60	2457826.53–2457847.24	1.957×10^{-3}
NGC 1367	53.76	−24.93	17.30	−19.76	−23.56	2457826.53–2457847.24	1.949×10^{-3}
NGC 6012	238.56	14.60	25.83	−19.76	−22.52	2457826.53–2457847.24	1.903×10^{-3}
NGC 1924	82.01	−5.31	28.84	−19.83	−22.96	2457826.53–2457847.24	1.882×10^{-3}
ESO 320-035	179.19	−38.19	27.04	−19.22	−21.87	2457826.53–2457847.24	1.875×10^{-3}
NGC 6181	248.09	19.83	33.57	−20.73	−23.96	2457826.53–2457847.24	1.833×10^{-3}
ESO 320-031	178.53	−39.87	38.18	−20.45	−24.87	2457826.53–2457847.24	1.791×10^{-3}
NGC 4444	187.15	−43.26	36.98	−20.63	−23.43	2457826.53–2457847.24	1.764×10^{-3}
NGC 1232	47.44	−20.58	14.52	−20.42	−23.43	2457826.53–2457847.24	1.756×10^{-3}
ESO 321-021	185.07	−40.39	39.65	−20.07	−22.64	2457826.53–2457847.24	1.667×10^{-3}
NGC 1425	55.55	−29.89	21.88	−20.36	−23.39	2457826.53–2457847.24	1.659×10^{-3}
NGC 1302	49.96	−26.06	19.59	−20.06	−23.63	2457826.53–2457847.24	1.646×10^{-3}
ESO 321-019	184.27	−39.05	37.64	−19.77	−22.82	2457826.53–2457847.24	1.638×10^{-3}
NGC 1309	50.53	−15.40	23.12	−19.92	−22.72	2457826.53–2457847.24	1.612×10^{-3}
NGC 6923	307.91	−30.83	37.15	−20.51	−24.04	2457826.53–2457847.24	1.604×10^{-3}
NGC 5956	233.74	11.75	26.28	−19.37	−22.23	2457826.53–2457847.24	1.601×10^{-3}
NGC 6010	238.58	0.54	25.35	−19.91	−23.09	2457826.53–2457847.24	1.589×10^{-3}
ESO 380-019	185.51	−35.79	38.02	−20.37	−24.24	2457826.53–2457847.24	1.538×10^{-3}
NGC 4219	184.11	−43.32	20.99	−20.51	−23.52	2457826.53–2457847.24	1.492×10^{-3}
NGC 1340	52.08	−31.07	19.77	−20.23	−24.08	2457826.53–2457847.24	1.481×10^{-3}
ESO 321-010	182.93	−38.55	38.02	−19.66	−22.79	2457826.53–2457847.24	1.474×10^{-3}
ESO 268-027	189.63	−42.86	38.42	−19.37	−22.45	2457826.53–2457847.24	1.367×10^{-3}
NGC 1354	53.12	−15.22	20.75	−19.20	−22.66	2457826.53–2457847.24	1.309×10^{-3}
IC 1151	239.63	17.44	24.21	−19.38	−21.51	2457826.53–2457847.24	1.257×10^{-3}
IC 5007	310.89	−29.70	32.66	−19.94	−22.46	2457826.53–2457847.24	1.256×10^{-3}
NGC 5951	233.43	15.01	25.94	−19.37	−22.02	2457826.53–2457847.24	1.207×10^{-3}
NGC 1843	78.53	−10.63	29.92	−19.22	−22.67	2457826.53–2457847.24	1.204×10^{-3}
IC 5039	310.81	−29.85	29.51	−19.85	−22.44	2457826.53–2457847.24	1.202×10^{-3}
UGC 03691	107.01	15.18	28.84	−20.00	−21.99	2457826.53–2457847.24	1.139×10^{-3}
PGC 012664	50.73	−11.20	34.67	−19.73	−21.10	2457826.53–2457847.24	1.018×10^{-3}
ESO 460-026	295.75	−27.42	18.11	−19.38	−21.96	2457826.53–2457847.24	9.656×10^{-4}

Table 9
(Continued)

Name (1)	R.A.(J2000) (2)	Decl.(J2000) (3)	Dist(Mpc) (4)	*B*(mag) (5)	*K*(mag) (6)	Obs_Window(JD) (7)	Score (8)
NGC 1350	52.78	−33.63	16.67	−19.95	−23.71	2457826.53–2457847.24	9.590×10^{-4}
UGC 10041	237.26	5.19	35.81	−19.27	−19.43	2457826.53–2457847.24	9.588×10^{-4}
ESO 322-020	187.30	−40.69	39.58	−19.39	−20.47	2457826.53–2457847.24	9.454×10^{-4}
NGC 4573	189.43	−43.62	37.42	−19.63	−23.22	2457826.53–2457847.24	8.463×10^{-4}
NGC 1289	49.71	−1.97	35.40	−19.89	−23.25	2457826.53–2457847.24	8.431×10^{-4}
NGC 1338	52.23	−12.15	32.36	−19.18	−22.54	2457826.53–2457847.24	7.990×10^{-4}
NGC 1406	54.85	−31.32	17.78	−19.35	−22.64	2457826.53–2457847.24	7.880×10^{-4}
NGC 1255	48.38	−25.73	17.70	−19.83	−22.86	2457826.53–2457847.24	7.629×10^{-4}
ESO 321-005	181.45	−38.85	36.46	−19.75	−22.20	2457826.53–2457847.24	7.583×10^{-4}
UGC 09977	235.50	0.71	31.33	−19.48	−21.88	2457826.53–2457847.24	7.198×10^{-4}
ESO 595-014	301.91	−21.13	29.92	−19.48	−22.38	2457826.53–2457847.24	6.539×10^{-4}
PGC 012633	50.57	−7.09	33.89	−19.24	−22.34	2457826.53–2457847.24	6.168×10^{-4}
PGC 017323	82.06	−16.12	25.35	−19.19	−20.84	2457826.53–2457847.24	6.044×10^{-4}
NGC 1292	49.56	−27.61	18.97	−19.19	−21.99	2457826.53–2457847.24	5.734×10^{-4}
NGC 3882	176.53	−56.39	23.12	−19.47	−23.71	2457826.53–2457847.24	5.256×10^{-4}
ESO 267-016	181.59	−44.45	39.26	−19.36	−22.30	2457826.53–2457847.24	5.193×10^{-4}
NGC 3149	150.93	−80.42	26.55	−19.49	−22.69	2457826.53–2457847.24	4.971×10^{-4}
IC 2006	58.62	−35.97	20.80	−19.32	−23.11	2457826.53–2457847.24	4.943×10^{-4}
UGC 03457	95.46	0.37	33.42	−19.66	−24.32	2457826.53–2457847.24	4.911×10^{-4}
ESO 019-006	169.05	−79.40	37.43	−19.29	−22.22	2457826.53–2457847.24	4.392×10^{-4}
PGC 090034	91.55	−0.54	25.35	−19.33	−22.07	2457826.53–2457847.24	4.061×10^{-4}
ESO 554-002	82.28	−19.93	36.21	−19.32	−20.30	2457826.53–2457847.24	3.974×10^{-4}
NGC 1179	45.66	−18.90	17.86	−19.26	−19.19	2457826.53–2457847.24	3.950×10^{-4}
NGC 4112	181.79	−40.21	34.67	−20.54	−23.50	2457826.53–2457847.24	3.886×10^{-4}

Note. The table columns provide the galaxy name, coordinates, distance, *B*- and *K*-band magnitudes, observing window, and the score from our ranking algorithm. The cumulative score is 0.370.

Table 10
Galaxies Observed after Trigger G284239

Name (1)	R.A.(J2000) (2)	Decl.(J2000) (3)	Dist(Mpc) (4)	*B*(mag) (5)	*K*(mag) (6)	Obs_Window(JD) (7)	Score (8)
NGC 6861	301.83	−48.37	28.05	−20.29	−24.53	2457877.13–2457892.23	6.452×10^{-2}
ESO 233-035	302.36	−48.28	33.97	−18.57	−22.23	2457877.13–2457892.23	6.320×10^{-2}
NGC 6861D	302.08	−48.21	33.42	−18.90	−23.42	2457877.13–2457892.23	6.280×10^{-2}
NGC 6868	302.48	−48.38	26.79	−20.45	−24.82	2457877.13–2457892.23	6.110×10^{-2}
NGC 6870	302.55	−48.29	33.42	−19.90	−23.67	2457877.13–2457892.23	6.030×10^{-2}
NGC 6861E	302.76	−48.69	33.90	−18.55	−21.04	2457877.13–2457892.23	4.919×10^{-2}
NGC 6851	300.89	−48.28	36.14	−20.13	−24.02	2457877.13–2457892.23	4.075×10^{-2}
NGC 6384	263.10	7.06	25.94	−21.26	−24.54	2457877.13–2457892.23	2.247×10^{-2}
NGC 6887	304.32	−52.80	30.06	−20.49	−23.52	2457877.13–2457892.23	2.239×10^{-2}
NGC 7083	323.94	−63.90	29.78	−20.77	−23.95	2457877.13–2457892.23	1.690×10^{-2}
NGC 7096	325.33	−63.91	35.81	−20.27	−23.82	2457877.13–2457892.23	1.420×10^{-2}
IC 5120	324.70	−64.35	37.33	−19.56	−22.06	2457877.13–2457892.23	1.417×10^{-2}
NGC 6889	304.72	−53.96	30.22	−19.49	−22.01	2457877.13–2457892.23	1.258×10^{-2}
IC 4837A	288.82	−54.13	33.42	−21.15	−24.47	2457877.13–2457892.23	1.258×10^{-2}
NGC 7191	331.72	−64.63	35.83	−19.96	−22.63	2457877.13–2457892.23	1.144×10^{-2}
NGC 7192	331.71	−64.32	37.84	−20.68	−24.38	2457877.13–2457892.23	1.119×10^{-2}
IC 4837	288.81	−54.67	33.42	−20.72	−20.38	2457877.13–2457892.23	1.088×10^{-2}
NGC 7140	328.06	−55.57	35.81	−21.01	−23.82	2457877.13–2457892.23	1.067×10^{-2}
IC 4839	288.89	−54.63	35.11	−20.02	−23.48	2457877.13–2457892.23	1.043×10^{-2}
IC 4889	296.31	−54.34	29.24	−20.33	−24.22	2457877.13–2457892.23	1.029×10^{-2}
IC 4888	296.22	−54.46	29.82	−18.29	−21.26	2457877.13–2457892.23	9.767×10^{-3}
ESO 107-015	318.43	−63.34	36.48	−19.20	−22.10	2457877.13–2457892.23	9.251×10^{-3}
NGC 7125	327.32	−60.71	36.98	−20.17	−22.63	2457877.13–2457892.23	9.043×10^{-3}
NGC 7126	327.33	−60.61	36.98	−19.82	−23.09	2457877.13–2457892.23	8.983×10^{-3}
NGC 6909	306.91	−47.03	35.48	−20.04	−23.53	2457877.13–2457892.23	8.959×10^{-3}
NGC 7219	333.28	−64.85	36.21	−19.88	−23.02	2457877.13–2457892.23	8.773×10^{-3}
IC 5084	317.31	−63.29	36.98	−19.50	−23.59	2457877.13–2457892.23	8.707×10^{-3}
UGC 10862	262.04	7.42	25.35	−19.22	−20.32	2457877.13–2457892.23	8.593×10^{-3}

Table 10
(Continued)

Name (1)	R.A.(J2000) (2)	Decl.(J2000) (3)	Dist(Mpc) (4)	*B*(mag) (5)	*K*(mag) (6)	Obs_Window(JD) (7)	Score (8)
NGC 6181	248.09	19.83	33.57	−20.73	−23.96	2457877.13–2457892.23	7.940×10^{-3}
NGC 6875A	302.98	−46.14	29.11	−19.52	−22.35	2457877.13–2457892.23	7.841×10^{-3}
IC 5092	319.06	−64.46	35.81	−20.17	−23.36	2457877.13–2457892.23	7.216×10^{-3}
NGC 6890	304.58	−44.81	31.19	−19.52	−23.44	2457877.13–2457892.23	6.834×10^{-3}
ESO 231-017	286.19	−47.85	35.14	−19.62	−23.20	2457877.13–2457892.23	6.820×10^{-3}
NGC 6788	291.71	−54.95	34.56	−21.09	−24.17	2457877.13–2457892.23	6.777×10^{-3}
ESO 108-023	334.13	−64.39	34.67	−19.33	−20.06	2457877.13–2457892.23	6.520×10^{-3}
NGC 7007	316.37	−52.55	34.67	−19.75	−23.74	2457877.13–2457892.23	6.482×10^{-3}
NGC 1625	69.28	−3.30	36.98	−20.44	−20.41	2457877.13–2457892.23	6.474×10^{-3}
NGC 6368	261.80	11.54	30.48	−20.62	−23.23	2457877.13–2457892.23	6.217×10^{-3}
NGC 7029	317.97	−49.28	38.37	−20.23	−24.38	2457877.13–2457892.23	5.843×10^{-3}
ESO 234-049	308.83	−49.87	31.19	−19.33	−21.87	2457877.13–2457892.23	5.789×10^{-3}
NGC 7041	319.13	−48.36	25.70	−20.06	−23.84	2457877.13–2457892.23	5.719×10^{-3}
ESO 235-085	319.57	−48.54	24.03	−18.53	−21.63	2457877.13–2457892.23	5.639×10^{-3}
ESO 186-062	308.51	−52.98	31.19	−19.10	−22.22	2457877.13–2457892.23	5.623×10^{-3}
IC 4986	304.30	−55.04	23.75	−19.08	−19.92	2457877.13–2457892.23	5.408×10^{-3}
NGC 7049	319.74	−48.56	29.92	−20.61	−25.13	2457877.13–2457892.23	5.378×10^{-3}
NGC 6810	295.89	−58.66	23.12	−20.42	−24.14	2457877.13–2457892.23	4.947×10^{-3}
IC 4821	287.38	−55.02	25.00	−18.98	−21.61	2457877.13–2457892.23	4.568×10^{-3}
NGC 7022	317.40	−49.30	29.49	−18.51	−22.12	2457877.13–2457892.23	4.554×10^{-3}
NGC 6902B	305.78	−43.87	34.67	−18.69	−20.75	2457877.13–2457892.23	4.340×10^{-3}
NGC 7205	332.14	−57.44	17.14	−19.87	−23.25	2457877.13–2457892.23	4.227×10^{-3}
IC 4946	305.99	−44.00	34.67	−20.12	−23.97	2457877.13–2457892.23	3.980×10^{-3}
IC 4797	284.12	−54.31	28.05	−20.23	−24.17	2457877.13–2457892.23	3.965×10^{-3}
NGC 6707	283.84	−53.82	33.42	−18.90	−22.97	2457877.13–2457892.23	3.426×10^{-3}
NGC 1665	72.07	−5.43	33.10	−19.32	−23.34	2457877.13–2457892.23	3.165×10^{-3}
ESO 183-030	284.23	−54.55	33.42	−20.11	−24.29	2457877.13–2457892.23	3.153×10^{-3}
IC 4901	298.60	−58.71	17.86	−19.61	−22.41	2457877.13–2457892.23	3.024×10^{-3}
NGC 6990	314.99	−55.56	25.36	−18.57	−21.08	2457877.13–2457892.23	2.858×10^{-3}
UGC 11030	268.64	2.88	27.67	−19.06	−19.63	2457877.13–2457892.23	2.152×10^{-3}
IC 4817	286.55	−56.16	33.42	−18.96	−21.27	2457877.13–2457892.23	2.013×10^{-3}
NGC 7059	321.84	−60.01	20.32	−18.62	−21.93	2457877.13–2457892.23	1.987×10^{-3}
UGC 03070	67.75	−2.00	30.65	−18.54	−20.39	2457877.13–2457892.23	1.847×10^{-3}
NGC 6509	269.86	6.29	27.67	−19.81	−22.48	2457877.13–2457892.23	1.807×10^{-3}
IC 5176	333.73	−66.85	26.42	−19.31	−23.37	2457877.13–2457892.23	1.799×10^{-3}
ESO 185-027	299.06	−56.91	23.81	−18.73	−21.94	2457877.13–2457892.23	1.782×10^{-3}
UGC 11093	270.47	6.97	21.18	−19.23	−22.25	2457877.13–2457892.23	1.732×10^{-3}
ESO 285-048	311.17	−45.98	28.18	−18.77	−21.33	2457877.13–2457892.23	1.670×10^{-3}
ESO 236-006	320.29	−47.52	28.93	−18.66	−19.52	2457877.13–2457892.23	1.648×10^{-3}
NGC 1637	70.37	−2.86	9.77	−18.54	−21.98	2457877.13–2457892.23	1.618×10^{-3}
IC 5249	341.78	−64.83	31.48	−19.52	−19.92	2457877.13–2457892.23	1.546×10^{-3}
ESO 235-001	312.26	−47.30	33.75	−18.51	−20.22	2457877.13–2457892.23	1.541×10^{-3}
NGC 6149	246.85	19.60	30.57	−18.65	−22.15	2457877.13–2457892.23	1.493×10^{-3}
PGC 015873	70.79	0.74	29.92	−18.41	−21.06	2457877.13–2457892.23	1.449×10^{-3}
UGC 03258	77.68	0.41	35.13	−19.59	−22.37	2457877.13–2457892.23	1.417×10^{-3}
ESO 340-010	304.36	−41.13	39.26	−18.82	−22.12	2457877.13–2457892.23	1.340×10^{-3}
ESO 146-001	329.09	−59.29	23.12	−18.28	−20.06	2457877.13–2457892.23	1.256×10^{-3}
ESO 340-032	306.73	−39.62	33.54	−18.98	−21.17	2457877.13–2457892.23	1.127×10^{-3}
NGC 7090	324.12	−54.56	6.28	−18.56	−20.83	2457877.13–2457892.23	1.097×10^{-3}
PGC 061359	271.09	7.28	28.11	−18.50	−23.01	2457877.13–2457892.23	1.041×10^{-3}
IC 4871	293.93	−57.52	22.59	−18.80	−20.88	2457877.13–2457892.23	8.689×10^{-4}
PGC 016060	72.14	−3.87	33.24	−18.36	−22.35	2457877.13–2457892.23	8.062×10^{-4}
ESO 286-063	317.47	−45.53	31.81	−19.21	−21.90	2457877.13–2457892.23	6.683×10^{-4}
IC 1151	239.63	17.44	24.21	−19.38	−21.51	2457877.13–2457892.23	5.755×10^{-4}
NGC 1507	61.11	−2.20	11.02	−18.41	−20.20	2457877.13–2457892.23	5.466×10^{-4}
UGC 02984	63.30	13.42	20.76	−18.55	−19.44	2457877.13–2457892.23	3.196×10^{-4}
IC 4885	295.97	−60.65	29.92	−18.39	−21.35	2457877.13–2457892.23	2.645×10^{-4}

Note. The table columns provide the galaxy name, coordinates, distance, *B*- and *K*-band magnitude, observing window, and the score from our ranking algorithm. The cumulative score is 0.846.

Table 11
Galaxies Observed after Trigger GW170814/G297595

Name (1)	R.A.(J2000) (2)	Decl.(J2000) (3)	Dist(Mpc) (4)	*B*(mag) (5)	*K*(mag) (6)	Obs_Window(JD) (7)	Score (8)
ESO 300-014	47.41	−41.03	10.86	−18.32	−16.32	2457980.28–2457982.25	4.898×10^{-2}
NGC 1255	48.38	−25.73	17.70	−19.83	−22.86	2457980.28–2457982.25	4.695×10^{-2}
ESO 481-018	49.64	−25.84	18.53	−18.28	−20.64	2457980.28–2457982.25	4.544×10^{-2}
NGC 0986	38.39	−39.05	23.12	−20.16	−24.04	2457980.28–2457982.25	4.508×10^{-2}
NGC 1201	46.03	−26.07	19.33	−20.01	−23.76	2457980.28–2457982.25	4.045×10^{-2}
NGC 1302	49.96	−26.06	19.59	−20.06	−23.63	2457980.28–2457982.25	4.039×10^{-2}
NGC 0908	35.77	−21.23	15.78	−20.53	−23.76	2457980.28–2457982.25	2.868×10^{-2}
PGC 013359	54.31	1.86	22.59	−19.15	−20.80	2457980.28–2457982.25	2.490×10^{-2}
NGC 1097	41.58	−30.27	14.19	−20.74	−24.51	2457980.28–2457982.25	2.430×10^{-2}
NGC 1232	47.44	−20.58	14.52	−20.42	−23.43	2457980.28–2457982.25	2.424×10^{-2}
NGC 1300	49.92	−19.41	14.52	−19.86	−23.25	2457980.28–2457982.25	2.200×10^{-2}
NGC 1292	49.56	−27.61	18.97	−19.19	−21.99	2457980.28–2457982.25	2.177×10^{-2}
NGC 1325	51.11	−21.54	19.95	−19.72	−22.87	2457980.28–2457982.25	2.159×10^{-2}
NGC 1297	49.81	−19.10	28.58	−19.68	−23.35	2457980.28–2457982.25	2.141×10^{-2}
NGC 1187	45.66	−22.87	18.36	−20.03	−23.22	2457980.28–2457982.25	1.612×10^{-2}
IC 1892	47.11	−23.06	34.67	−18.85	−19.74	2457980.28–2457982.25	1.418×10^{-2}
ESO 545-005	35.03	−19.75	30.20	−19.15	−21.80	2457980.28–2457982.25	1.314×10^{-2}
IC 1898	47.58	−22.41	19.50	−18.39	−21.41	2457980.28–2457982.25	1.057×10^{-2}
PGC 1075354	52.68	−3.16	24.72	−18.94	−21.05	2457980.28–2457982.25	9.864×10^{-3}
NGC 1309	50.53	−15.40	23.12	−19.92	−22.72	2457980.28–2457982.25	9.671×10^{-3}
PGC 012664	50.73	−11.20	34.67	−19.73	−21.10	2457980.28–2457982.25	7.206×10^{-3}
PGC 012633	50.57	−7.09	33.89	−19.24	−22.34	2457980.28–2457982.25	4.823×10^{-3}
NGC 1337	52.03	−8.39	11.91	−18.86	−21.16	2457980.28–2457982.25	4.248×10^{-3}
NGC 0988	38.87	−9.36	17.30	−18.98	−24.19	2457980.28–2457982.25	3.882×10^{-3}

Note. The table columns provide the galaxy name, coordinates, distance, *B*- and *K*-band magnitudes, observing window, and the score from our ranking algorithm. The cumulative score is 0.550.

Table 12
Galaxies Observed after Trigger GRB 170817a

Name (1)	R.A.(J2000) (2)	Decl.(J2000) (3)	Dist(Mpc) (4)	*B*(mag) (5)	*K*(mag) (6)	Obs_Window(JD) (7)
NGC 3749	173.97	−38.00	38.02	−20.80	−24.20	2457980.28–2457982.25
NGC 3269	157.49	−35.22	36.40	−20.86	−23.75	2457980.28–2457982.25
NGC 3273	157.62	−35.61	36.98	−18.99	−23.91	2457980.28–2457982.25
NGC 3281C	158.25	−34.89	37.29	−18.79	−22.62	2457980.28–2457982.25
ESO 268-003	186.32	−43.45	37.92	−18.95	−23.22	2457980.28–2457982.25
ESO 443-042	195.87	−29.83	33.42	−19.69	−22.94	2457980.28–2457982.25
ESO 440-004	176.42	−28.37	22.93	−18.82	−18.47	2457980.28–2457982.25
IC 4180	196.74	−23.92	33.65	−19.98	−23.04	2457980.28–2457982.25
ESO 508-015	197.33	−24.38	33.42	−18.77	−18.79	2457980.28–2457982.25
NGC 4806	194.05	−29.50	28.84	−19.26	−21.96	2457980.28–2457982.25
NGC 3717	172.88	−30.31	16.90	−19.94	−23.62	2457980.28–2457982.25
NGC 3585	168.32	−26.75	20.05	−20.77	−24.81	2457980.28–2457982.25
NGC 5365A	209.16	−44.01	36.98	−20.27	−24.00	2457980.28–2457982.25
ESO 507-008	191.42	−26.63	33.19	−19.67	−20.51	2457980.28–2457982.25
NGC 5161	202.31	−33.17	18.53	−19.84	−22.71	2457980.28–2457982.25
NGC 5042	198.88	−23.98	12.65	−18.70	−21.11	2457980.28–2457982.25
ESO 572-049	180.85	−19.52	31.62	−18.57	−19.95	2457980.28–2457982.25
ESO 126-025	144.64	−61.74	34.42	−19.89	−23.34	2457980.28–2457982.25
NGC 4856	194.84	−15.04	11.54	−18.95	−22.84	2457980.28–2457982.25
ESO 576-003	197.65	−21.75	28.44	−18.94	−20.65	2457980.28–2457982.25
IC 2539	151.07	−31.36	30.76	−19.53	−22.39	2457980.28–2457982.25
ESO 435-015	149.46	−31.01	32.36	−18.35	−21.04	2457980.28–2457982.25
ESO 176-006	224.29	−54.39	38.01	−21.52	−24.43	2457980.28–2457982.25
ESO 435-010	149.09	−31.30	33.28	−18.68	−19.91	2457980.28–2457982.25
ESO 092-014	152.72	−66.65	23.96	−19.28	−23.28	2457980.28–2457982.25
NGC 5119	201.00	−12.28	35.19	−18.98	−23.08	2457980.28–2457982.25
NGC 3952	178.42	−4.00	23.12	−19.62	−20.81	2457980.28–2457982.25
NGC 5670	218.90	−45.97	36.98	−19.24	−24.23	2457980.28–2457982.25
NGC 3915	177.23	−4.68	36.06	−18.51	−21.04	2457980.28–2457982.25

Table 12
(Continued)

Name (1)	R.A.(J2000) (2)	Decl.(J2000) (3)	Dist(Mpc) (4)	*B*(mag) (5)	*K*(mag) (6)	Obs_Window(JD) (7)
NGC 4546	188.87	−3.79	14.06	−19.50	−23.35	2457980.28–2457982.25
ESO 097-013	213.29	−65.34	4.21	−19.03	−23.14	2457980.28–2457982.25

Note. The table columns provide the galaxy name, coordinates, distance, *B*- and *K*-band magnitudes, and the observing window. For the GRB trigger, we selected the 31 most luminous galaxies in the 90% Fermi region (Valenti et al. 2017).

Table 13
Galaxies Observed after Trigger GW170817/G298048

Name (1)	R.A.(J2000) (2)	Decl.(J2000) (3)	Dist(Mpc) (4)	*B*(mag) (5)	*K*(mag) (6)	Obs_Window(JD) (7)	Score (8)	Score2 (9)
NGC 4993	197.45	−23.38	39.99	−20.20	−23.42	2457983.41–2457985.17	1.195×10^{-1}	1.615×10^{-1}
IC 4197	197.02	−23.80	34.10	−20.24	−23.39	2457983.41–2457985.17	1.346×10^{-1}	1.386×10^{-1}
ESO 508-019	197.47	−24.24	38.55	−19.33	−21.16	2457983.41–2457985.17	1.060×10^{-1}	1.311×10^{-1}
NGC 4968	196.77	−23.68	33.42	−19.44	−23.14	2457983.41–2457985.17	1.145×10^{-1}	1.103×10^{-1}
ESO 508-024	197.69	−23.87	33.42	−19.98	−21.59	2457983.41–2457985.17	9.862×10^{-2}	1.021×10^{-1}
IC 4180	196.74	−23.92	33.65	−19.98	−23.04	2457983.41–2457985.17	9.361×10^{-2}	9.230×10^{-2}
ESO 508-015	197.33	−24.38	33.42	−18.77	−18.79	2457983.41–2457985.17	8.194×10^{-2}	7.894×10^{-2}
ESO 508-004	196.72	−22.84	33.96	−18.33	−18.75	2457983.41–2457985.17	7.466×10^{-2}	7.586×10^{-2}
ESO 508-003	196.60	−24.16	33.43	−19.20	−21.23	2457983.41–2457985.17	5.371×10^{-2}	5.180×10^{-2}
ESO 575-053	196.27	−22.38	30.48	−18.44	−21.31	2457983.41–2457985.17	2.850×10^{-2}	1.897×10^{-2}
IC 0874	199.75	−27.63	29.06	−19.29	−22.64	2457983.41–2457985.17	1.873×10^{-2}	9.936×10^{-3}
ESO 576-001	197.60	−21.68	35.47	−19.18	−22.00	2457983.41–2457985.17	7.000×10^{-3}	8.057×10^{-3}
NGC 5078	199.96	−27.41	27.67	−21.24	−25.09	2457983.41–2457985.17	1.685×10^{-2}	6.943×10^{-3}
NGC 5061	199.52	−26.84	24.21	−20.82	−24.63	2457983.41–2457985.17	1.935×10^{-2}	3.727×10^{-3}
ESO 576-003	197.65	−21.75	28.44	−18.94	−20.65	2457983.41–2457985.17	6.816×10^{-3}	3.242×10^{-3}
ESO 508-051	200.12	−26.08	34.04	−18.41	−19.55	2457983.41–2457985.17	1.878×10^{-3}	1.922×10^{-3}
NGC 5101	200.44	−27.43	24.21	−20.68	−24.76	2457983.41–2457985.17	6.919×10^{-3}	1.333×10^{-3}
NGC 4680	191.73	−11.64	29.92	−19.12	−22.61	2457983.41–2457985.17	1.299×10^{-3}	7.933×10^{-4}
ESO 576-005	197.83	−19.83	38.54	−19.04	−20.21	2457983.41–2457985.17	4.122×10^{-3}	3.943×10^{-4}
NGC 4663	191.20	−10.20	30.40	−18.75	−22.71	2457983.41–2457985.17	5.385×10^{-3}	3.534×10^{-4}

Note. The table columns provide the galaxy name, coordinates, distance, *B*- and *K*-band magnitudes, observing window, and the score from our ranking algorithm. It is shown that NGC 4993, which is the host galaxy of the kilonova AT17fgo, is ranked by our algorithm as the second in the list; see column "Score." After taking into account the distance distribution from GW estimation, NGC 4993 is the highest ranking galaxy, shown as column "score2." The galaxy list is ranked with "score2."

Table 14
Galaxies Observed after Trigger G299232

Name (1)	R.A.(J2000) (2)	Decl.(J2000) (3)	Dist(Mpc) (4)	*B*(mag) (5)	*K*(mag) (6)	Obs_Window(JD) (7)	Score (8)
NGC 0772	29.83	19.01	32.36	−21.78	−25.35	2457991.48–2458005.21	5.598×10^{-2}
NGC 0524	21.20	9.54	23.99	−20.53	−24.74	2457991.48–2458005.21	5.373×10^{-2}
NGC 0770	29.81	18.95	32.36	−18.75	−22.27	2457991.48–2458005.21	5.272×10^{-2}
NGC 0518	21.07	9.33	30.31	−19.35	−22.61	2457991.48–2458005.21	5.084×10^{-2}
NGC 0525	21.22	9.70	22.32	−18.32	−21.14	2457991.48–2458005.21	5.020×10^{-2}
NGC 0516	21.03	9.55	29.87	−18.82	−21.86	2457991.48–2458005.21	4.811×10^{-2}
NGC 0532	21.32	9.26	29.92	−19.73	−23.55	2457991.48–2458005.21	4.614×10^{-2}
IC 0101	21.04	9.93	30.71	−18.40	−20.56	2457991.48–2458005.21	4.544×10^{-2}
NGC 0522	21.19	9.99	29.92	−19.23	−22.94	2457991.48–2458005.21	4.246×10^{-2}
NGC 0502	20.73	9.05	30.67	−19.27	−22.70	2457991.48–2458005.21	4.122×10^{-2}
NGC 0489	20.47	9.21	29.92	−20.12	−22.82	2457991.48–2458005.21	3.494×10^{-2}
NGC 0488	20.45	5.26	29.92	−21.41	−25.42	2457991.48–2458005.21	2.466×10^{-2}
NGC 6925	308.59	−31.98	28.31	−21.07	−24.27	2457991.48–2458005.21	2.074×10^{-2}
NGC 0628	24.17	15.78	7.31	−19.53	−22.47	2457991.48–2458005.21	1.475×10^{-2}
IC 1711	22.73	17.19	35.81	−19.20	−23.23	2457991.48–2458005.21	1.345×10^{-2}
ESO 340-012	304.64	−39.34	33.42	−19.15	−21.25	2457991.48–2458005.21	1.189×10^{-2}
UGC 01020	21.68	17.26	30.71	−19.02	−21.32	2457991.48–2458005.21	1.182×10^{-2}
ESO 340-017	304.92	−39.29	34.44	−20.14	−21.75	2457991.48–2458005.21	1.125×10^{-2}
NGC 0474	20.03	3.42	29.92	−20.44	−23.82	2457991.48–2458005.21	1.107×10^{-2}

Table 14
(Continued)

Name (1)	R.A.(J2000) (2)	Decl.(J2000) (3)	Dist(Mpc) (4)	B(mag) (5)	K(mag) (6)	Obs_Window(JD) (7)	Score (8)
UGC 00958	21.14	16.54	28.87	−18.81	−18.31	2457991.48–2458005.21	1.047×10^{-2}
NGC 0520	21.14	3.79	29.92	−20.39	−24.01	2457991.48–2458005.21	1.002×10^{-2}
NGC 0470	19.94	3.41	36.14	−20.42	−23.95	2457991.48–2458005.21	9.803×10^{-3}
NGC 0514	21.02	12.92	23.99	−19.59	−22.76	2457991.48–2458005.21	9.406×10^{-3}
ESO 340-009	304.34	−38.67	29.65	−18.71	−19.96	2457991.48–2458005.21	9.200×10^{-3}
NGC 0473	19.98	16.54	29.92	−19.78	−22.82	2457991.48–2458005.21	9.118×10^{-3}
UGC 01197	25.64	18.31	35.16	−18.53	−19.97	2457991.48–2458005.21	8.382×10^{-3}
IC 5013	307.14	−36.03	29.92	−19.99	−23.77	2457991.48–2458005.21	5.874×10^{-3}
NGC 0660	25.76	13.64	9.25	−19.04	−22.49	2457991.48–2458005.21	5.767×10^{-3}
ESO 399-025	303.37	−37.19	33.40	−19.29	−22.62	2457991.48–2458005.21	5.604×10^{-3}
ESO 400-026	307.04	−35.81	31.71	−18.55	−19.15	2457991.48–2458005.21	5.589×10^{-3}
UGC 00903	20.45	17.59	29.92	−18.74	−22.96	2457991.48–2458005.21	5.541×10^{-3}
NGC 0485	20.36	7.02	29.92	−18.99	−21.56	2457991.48–2458005.21	4.800×10^{-3}
UGC 01110	23.32	13.33	33.73	−18.51	−20.54	2457991.48–2458005.21	4.575×10^{-3}
UGC 00964	21.15	7.72	37.84	−18.45	−20.98	2457991.48–2458005.21	4.571×10^{-3}
NGC 6923	307.91	−30.83	37.15	−20.51	−24.04	2457991.48–2458005.21	4.456×10^{-3}
ESO 340-008	304.30	−40.92	33.42	−19.15	−20.75	2457991.48–2458005.21	4.073×10^{-3}
ESO 462-031	307.97	−30.80	33.92	−18.62	−21.43	2457991.48–2458005.21	4.012×10^{-3}
PGC 004612	19.18	16.40	28.90	−18.37	−21.15	2457991.48–2458005.21	3.910×10^{-3}
PGC058798	250.51	−5.03	19.95	−19.07	−22.34	2457991.48–2458005.21	3.082×10^{-3}
NGC 6106	244.70	7.41	24.66	−19.60	−22.34	2457991.48–2458005.21	3.047×10^{-3}
ESO 340-032	306.73	−39.62	33.54	−18.98	−21.17	2457991.48–2458005.21	1.958×10^{-3}

Note. The table columns provide the galaxy name, coordinates, distance, B- and K-band magnitudes, observing window, and the score from our ranking algorithm. The cumulative score is 0.775.

ORCID iDs

Sheng Yang https://orcid.org/0000-0002-2898-6532
David J. Sand https://orcid.org/0000-0003-4102-380X
Stefano Valenti https://orcid.org/0000-0001-8818-0795
Enrico Cappellaro https://orcid.org/0000-0001-5008-8619
Leonardo Tartaglia https://orcid.org/0000-0003-3433-1492
Alessandra Corsi https://orcid.org/0000-0001-8104-3536
Daniel E. Reichart https://orcid.org/0000-0002-5060-3673

References

Aasi, J., Abadie, J., Abbott, B. P., et al. 2015, CQGra, 32, 115012
Abbott, B. P., Abbott, R., Abbott, T. D., et al. 2016a, PhRvL, 116, 061102
Abbott, B. P., Abbott, R., Abbott, T. D., et al. 2016b, PhRvL, 116, 241103
Abbott, B. P., Abbott, R., Abbott, T. D., et al. 2016c, PhRvX, 6, 041015
Abbott, B. P., Abbott, R., Abbott, T. D., et al. 2016d, ApJL, 826, L13
Abbott, B. P., Abbott, R., Abbott, T. D., et al. 2017a, PhRvL, 119, 161101
Abbott, B. P., Abbott, R., Abbott, T. D., et al. 2017b, ApJL, 848, L12
Abbott, B. P., Abbott, R., Abbott, T. D., et al. 2017c, PhRvL, 118, 221101
Abbott, B. P., Abbott, R., Abbott, T. D., et al. 2017d, PhRvL, 119, 141101
Abbott, B. P., Abbott, R., Abbott, T. D., et al. 2018, LRR, 21, 3
Abbott, B. P. & The LIGO Scientific Collaboration 2016e, LRR, 19, 1
Acernese, F., Agathos, M., Agatsuma, K., et al. 2015, CQGra, 32, 024001
Arcavi, I., Hosseinzadeh, G., Howell, D. A., et al. 2017a, Natur, 551, 64
Arcavi, I., McCully, C., Hosseinzadeh, G., et al. 2017b, ApJL, 848, L33
Astropy Collaboration, Price-Whelan, A. M., Sipőcz, B. M., et al. 2018, AJ, 156, 123
Barnes, J., & Kasen, D. 2013, ApJ, 775, 18
Bartos, I., Kocsis, B., Haiman, Z., & Márka, S. 2017, ApJ, 835, 165
Becker, A. 2015, HOTPANTS: High Order Transform of PSF ANd Template Subtraction, Astrophysics Source Code Library, ascl:1504.004
Bertin, E., & Arnouts, S. 1996, A&AS, 117, 393
Brown, T. M., Baliber, N., Bianco, F. B., et al. 2013, PASP, 125, 1031
Connaughton, V., Burns, E., Goldstein, A., et al. 2016, ApJL, 826, L6
Coulter, D. A., Foley, R. J., Kilpatrick, C. D., et al. 2017, Sci, 358, 1556
Dálya, G., Galgóczi, G., Dobos, L., et al. 2018, MNRAS, 479, 2374
de Mink, S. E., & King, A. 2017, ApJL, 839, L7
Doctor, Z., Kessler, R., Herner, K., et al. 2019, ApJL, 873, L24
Evans, P. A., Cenko, S. B., Kennea, J. A., et al. 2017, Sci, 358, 1565
Fan, X., Messenger, C., & Heng, I. S. 2014, ApJ, 795, 43
Firth, R. E., Sullivan, M., Gal-Yam, A., et al. 2015, MNRAS, 446, 3895
Fong, W., & Berger, E. 2013, ApJ, 776, 18
Gehrels, N., Cannizzo, J. K., Kanner, J., et al. 2016, ApJ, 820, 136
Goldstein, A., Veres, P., Burns, E., et al. 2017, ApJL, 848, L14
Górski, K. M., Hivon, E., Banday, A. J., et al. 2005, ApJ, 622, 759
Haggard, D., Nynka, M., Ruan, J. J., et al. 2017, ApJL, 848, L25
Hallinan, G., Corsi, A., Mooley, K. P., et al. 2017, Sci, 358, 1579
Hosseinzadeh, G., Sand, D. J., Valenti, S., et al. 2017, ApJL, 845, L11
Kasen, D., Badnell, N. R., & Barnes, J. 2013, ApJ, 774, 25
Kasen, D., Metzger, B., Barnes, J., Quataert, E., & Ramirez-Ruiz, E. 2017, Natur, 551, 80
Kasliwal, M. M., Cenko, S. B., Singer, L. P., et al. 2016, ApJL, 824, L24
Li, L.-X., & Paczyński, B. 1998, ApJL, 507, L59
LIGO Scientific Collaboration &Virgo Collaboration 2017a, GCN, 20763
LIGO Scientific Collaboration &Virgo Collaboration 2017b, GCN, 20364
LIGO Scientific Collaboration &Virgo Collaboration 2017c, GCN, 20486
LIGO Scientific Collaboration &Virgo Collaboration 2017d, GCN, 21281
LIGO Scientific Collaboration &Virgo Collaboration 2017e, GCN, 20689
LIGO Scientific Collaboration &Virgo Collaboration 2017f, GCN, 21284
LIGO Scientific Collaboration &Virgo Collaboration 2017g, GCN, 20738
LIGO Scientific Collaboration &Virgo Collaboration 2017h, GCN, 20840
LIGO Scientific Collaboration &Virgo Collaboration 2017i, GCN, 20833
LIGO Scientific Collaboration &Virgo Collaboration 2017j, GCN, 20860
LIGO Scientific Collaboration &Virgo Collaboration 2017k, GCN, 21060
LIGO Scientific Collaboration &Virgo Collaboration 2017l, GCN, 21221
LIGO Scientific Collaboration &Virgo Collaboration 2017m, GCN, 21431
LIGO Scientific Collaboration &Virgo Collaboration 2017n, GCN, 21474
LIGO Scientific Collaboration &Virgo Collaboration 2017o, GCN, 21510
LIGO Scientific Collaboration &Virgo Collaboration 2017p, GCN, 21513
LIGO Scientific Collaboration &Virgo Collaboration 2017q, GCN, 21505
LIGO Scientific Collaboration &Virgo Collaboration 2017r, GCN, 21656
LIGO Scientific Collaboration &Virgo Collaboration 2017s, GCN, 21600
LIGO Scientific Collaboration &Virgo Collaboration 2017t, GCN, 21693
LIGO Scientific Collaboration &Virgo Collaboration 2019, arXiv:1901.03310
Lipunov, V. M., Gorbovskoy, E., Kornilov, V. G., et al. 2017, ApJL, 850, L1
Loeb, A. 2016, ApJL, 819, L21
Margutti, R., Berger, E., Fong, W., et al. 2017, ApJL, 848, L20

Marion, G. H., Brown, P. J., Vinkó, J., et al. 2016, ApJ, 820, 92
Metzger, B. D. 2017, LRR, 20, 3
Metzger, B. D., Martínez-Pinedo, G., Darbha, S., et al. 2010, MNRAS, 406, 2650
Nitz, A. H., Dal Canton, T., Davis, D., & Reyes, S. 2018, PhRvD, 98, 024050
Perna, R., Chruslinska, M., Corsi, A., & Belczynski, K. 2018, MNRAS, 477, 4228
Perna, R., Lazzati, D., & Giacomazzo, B. 2016, ApJL, 821, L18
Pian, E., D'Avanzo, P., Benetti, S., et al. 2017, Natur, 551, 67
Piran, T., Nakar, E., & Rosswog, S. 2013, MNRAS, 430, 2121
Reichart, D., Nysewander, M., Moran, J., et al. 2005, NCimC, 28, 767
Sand, D. J., Graham, M. L., Botyánszki, J., et al. 2018, ApJ, 863, 24
Savchenko, V., Ferrigno, C., Kuulkers, E., et al. 2017, ApJL, 848, L15
Singer, L. P., Chen, H.-Y., Holz, D. E., et al. 2016, ApJL, 829, L15
Singer, L. P., & Price, L. R. 2016, PhRvD, 93, 024013
Smartt, S. J., Chambers, K. C., Smith, K. W., et al. 2016, MNRAS, 462, 4094
Soares-Santos, M., Holz, D. E., Annis, J., et al. 2017, ApJL, 848, L16
Tanvir, N. R., Levan, A. J., González-Fernández, C., et al. 2017, ApJL, 848, L27
Tartaglia, L., Sand, D. J., Valenti, S., et al. 2018, ApJ, 853, 62
Troja, E., Piro, L., van Eerten, H., et al. 2017, Natur, 551, 71
Valenti, S., Sand, D. J., Yang, S., et al. 2017, ApJL, 848, L24
van Eerten, H. J., & MacFadyen, A. I. 2011, ApJL, 733, L37
Veitch, J., Raymond, V., Farr, B., et al. 2015, PhRvD, 91, 042003
Villar, V. A., Guillochon, J., Berger, E., et al. 2017, ApJL, 851, L21
White, D. J., Daw, E. J., & Dhillon, V. S. 2011, CQGra, 28, 085016
Wright, D. E., Smartt, S. J., Smith, K. W., et al. 2015, MNRAS, 449, 451
Yang, S., Valenti, S., Cappellaro, E., et al. 2017, ApJL, 851, L48
Yang, S., Valenti, S., Sand, D., et al. 2017a, GCN, 20669
Yang, S., Valenti, S., Sand, D., et al. 2017b, GCN, 20875
Yang, S., Valenti, S., Sand, D., et al. 2017c, GCN, 21010
Yang, S., Valenti, S., Sand, D., et al. 2017d, GCN, 20876
Yang, S., Valenti, S., Sand, D., et al. 2017e, GCN, 21009
Yang, S., Valenti, S., Sand, D., et al. 2017f, GCN, 21116
Yang, S., Valenti, S., Sand, D., et al. 2017g, GCN, 21878
Yang, S., Valenti, S., Sand, D., et al. 2017h, GCN, 21531
Yang, S., Valenti, S., Sand, D., et al. 2017i, GCN, 21539
Yang, S., Valenti, S., Sand, D., et al. 2017j, GCN, 21579
Yuan, F., Jerkstrand, A., Valenti, S., et al. 2016, MNRAS, 461, 2003
Zhang, S.-N., Liu, Y., Yi, S., Dai, Z., & Huang, C. 2016, arXiv:1604.02537